COVID-19 Puzzles: A Resolution*

Tony Berrada[†], Jerome Detemple[‡], and Marcel Rindisbacher[§]

November 1, 2022

Abstract

This paper examines the economic impact of COVID-19 in an equilibrium framework. Our model, BDRA-SSL, combines two ingredients: (i) beliefs-dependent preferences for economic dynamics and (ii) stochastic SEIRD model with unpredictable birth and vaccine discovery events, and mitigating policy and behavioral responses, for disease propagation. We estimate the model based on economic time series and COVID-19 data. We show it explains the behaviors and levels of the S&P 500, the index volatility, and the number of new cases during the recent outbreak, while providing a good match for 25 unconditional moments of economic time series. Beliefs-dependence emerges as a critical ingredient for this comprehensive explanation of short term dynamics during the COVID-19 outbreak and of long run statistical properties. A comparison study establishes the performance of BDRA-SSL versus alternative specifications.

JEL Classification: G13.

Key Words: COVID-19, SEIRD, shelter-in-place, jumps, beliefs-dependent preferences, stock market, equity premium, volatility, correlation, consumption, unemployment.

*This paper was presented at Soochow University (Suzhou), FEBS 2022, EFMA 2022, WFC 2022, and won the Best Paper award at WFC 2022. We thank Matthias Lassak and seminar participants for comments.

[†]Geneva Finance Research Institute, University of Geneva, Bd. du Pont d'Arve 40, CH-1211 Geneva 4, Switzerland. Email: Tony.Berrada@unige.ch

[‡]Questrom School of Business, Boston University, 595 Commonwealth Ave., Boston, MA 02215, United States. Email: detemple@bu.edu

[§]Questrom School of Business, Boston University, 595 Commonwealth Ave., Boston, MA 02215, United States. Email: rindisbm@bu.edu

1. Introduction

The COVID-19 outbreak challenges economic theory on several grounds. It is characterized by a sharp decline in the consumption growth rate followed by a quick reversal. It features a rapidly declining stock market followed by a slower increase to levels commensurate with initial values. It displays episodes of large and fluctuating volatility in the market. This paper seeks to explain the magnitudes and patterns of these short run empirical regularities in an integrated epidemic-economy model consistent with moment properties of long run economic time series.

The outbreak took markets across the world by surprise. Although data from China showed clear and early evidence of rapid propagation and associated economic damage, markets initially failed to react, discounting the possibility of contagion across regions and continents. The rapid decrease in the US market, for instance, began on February 20, several months after the epidemic started to rage in China. The S&P500 reached its trough on March 23, about 30% below average levels during the first two months of 2020. The index took nearly 5 months to recover its February 20 level. In parallel, the VIX, a measure of market volatility, went from 15.56 on February 20 to a peak of 82.69 on March 16. It then progressively decreased to 24.52 on June 5, before spiking at 40.79 on June 11. A second spike occurred on September 3 following a short-lived downward adjustment. It has since evolved in the 15-40 range. Markets in other countries have experienced similar patterns although at different dates and over different periods.

The goal of this paper is to explain these phenomena, more specifically levels and patterns that have characterized US markets. A key question is whether the empirical evidence associated with COVID-19 is consistent with the predictions of a "finely-tuned" asset pricing model. By finely-tuned, we mean an asset pricing model explaining the long run behavior of financial markets, i.e., outside epidemic states. Given such a model, questions pertaining to the origins of economic fluctuations can be addressed. Are level adjustment patterns and volatility bursts the result of certain policy decisions or of natural disease propagation mechanisms? Do they reflect behavioral responses of economic agents? Are they tied to events unrelated to COVID-

19? Answers to these question may help to provide perspective on the scope and effectiveness of policy making.

For these purposes, we use the model with beliefs-dependent risk aversion (BDRA) in Berrada, Detemple and Rindisbacher (2018) as a starting point. This choice is motivated by the overall performance, static and dynamic, of the model. On the static front it provides a good match for 25 moment condition, e.g., unconditional estimates of the equity premium, log price-dividend ratio (PDR), stock market volatility and correlations between log PDR and growth rate of consumption. On the dynamic front it has attractive properties, e.g., spikes in model-implied recession probabilities coincide with NBER recession periods, model volatility tracks realized volatility, and the equity premium displays countercyclical behavior.

First, we extend the model to incorporate short term dynamics associated with a pandemic. This extension accounts for the unpredictable nature of pandemic events and vaccine discoveries, mitigating governmental policies, and social distancing responses. Pandemic uncertainty is modelled through a non-recurrent Markov chain with three possible regimes: no pandemic, pandemic and vaccine. It is injected into the benchmark pandemic model employed, the SEIRD model.[1] Mitigating government policy takes the form of mandates to shelter-in-place (SIP) and terminations thereof (LIFT). Social distancing responses take the form of variations in the transmission rate of the disease at certain times including policy change dates. The combined model is called the BDRA-SSL model, i.e., BDRA with SEIRD pandemic propagation and SIP-LIFT policy response. Of particular note is the fact that BDRA-SSL produces closed form solutions for equilibrium quantities, including stock prices and volatilities, in spite of the unpredictability associated with the pandemic uncertainty and the complexities of policy and social responses.

Second, we estimate the model based on COVID-19 data, S&P 500 level and volatility data and time series for consumption, dividends, macro aggregates and others. Estimation is carried out in two stages. In the first stage, the pre-pandemic stage, the economic model is

[1]More complex propagation mechanisms can be substituted without affecting the solution procedure and the main structural results.

estimated based on 25 moment conditions. Relative to prior literature relying on the BDRA model, the estimation uses an augmented data set from 1957 to 2019. In the second stage, the pandemic stage, the disease propagation parameters and the parameters governing its effects on consumption, dividend and unemployment are estimated. Estimation is carried out so as to minimize the mean squared distance between model-implied and observed trajectories of the S&P 500 level, index volatility, and number of new COVID-19 cases. The data set used for that purpose goes from January 1, 2020 to August 7, 2020.

Third, we document the performance of the BDRA-SSL model. There are two aspects. We first show that the model performs well regarding the quantities that were targeted in the estimation. Model-implied variables and statistics are close to their empirical counterparts, both during the pre-pandemic period and the early stages of the outbreak. Pre-pandemic, the estimated model provides a good fit for 25 targeted moment conditions, confirming the results in Detemple et al (2018) for the longer data set. Intra-pandemic, it closely matches the number of new cases and the levels of volatility recorded during the COVID-19 outbreak, and it displays the asymmetric V-shape pattern of the S&P 500 while providing good matches for the index size and the timing of variations. Next, we document the reasons behind the model's performance. At the core is the behavior of the model-implied recession probability. It increases during the COVID-19 recession period declared by the NBER, but decreases immediately thereafter, thus explaining the ability to capture sharp variations in the data. Crucially, BDRA is a necessary ingredient for explaining the empirical patterns.

Fourth, the paper compares performance across models. Alternatives examined are the nested specifications BDRA (without pandemic component), CRRA-SSL (constant relative risk aversion), BDRA-SSL-C (constrained version of BDRA-SSL), and the non-nested model BDRA-SIRD-SL (with SIRD pandemic propagation). It shows that standalone BDRA, without feedback effects from an epidemic component, is unable to explain patterns and magnitudes. It also shows that the standard CRRA model augmented by the same SEIRD epidemic propagation model with SIP-LIFT policy response (CRRA-SSL) performs poorly. Model specification tests reject the nested alternatives BDRA, CRRA-SSL and BDRA-SSL-C. Model selection criteria show BDRA-SSL dominates all nested specifications as well as the non-nested BDRA-SIRD-SL model. It also performs best pre-pandemic based on 25 moment conditions. Hence, BDRA-SSL dominates alternatives in terms of simultaneously fitting short term and long term properties of the data.

The paper relates to three branches of the literature. First, it generalizes recent contributions seeking to examine the impact of pandemics on equilibrium asset prices, e.g., Detemple (2022). It differs in that it (i) integrates an epidemiology propagation model into the model with BDRA preferences, (ii) allows for unpredictable events such as the outbreak of a pandemic and the discovery of a vaccine, (iii) includes volatility and correlations in the analysis and focuses not only on patterns but also levels, and (iv) estimates a version of the model allowing for time-dependent contamination rate and examines its performance. The estimated model fits the data well: on the economic front, it explains the levels and adjustment patterns of the S&P 500 index and its volatility, during the COVID-19 outbreak.

Second, it contributes to the general equilibrium asset pricing literature. It extends, in particular, the BDRA model in Berrada, Detemple and Rindisbacher (2018) showing that market value and volatility inherit new components tied to the likelihood of occurrence of an outbreak and the likelihood of a vaccine discovery. Equilibrium formulas obtained are explicit allowing for estimation and straightforward simulation. It also complements earlier studies such as Merton (1973), Breeden (1979) and Cox, Ingersoll and Ross (1985), by incorporating an unexpected epidemic phenomenon into an equilibrium valuation framework.

Third, it connects to the growing literature dealing with the COVID-19 outbreak. Recent contributions have documented the empirical impact on the market, e.g., Gorsuch and Koijen (2020) and volatility, e.g., Cheng (2020). The present paper explains this empirical evidence, along with other aspects, in an equilibrium setting. It shows in particular that BDRA is essential for rationalizing the data. Other recent articles examine the role and impact of mitigation policies, e.g., Eichenbaum et al (2021), Jones et al (2021) and Hong et al (2021). The first study investigates the implications of individual decisions and government policies for disease propagation mechanisms and economic aggregates dynamics. The second one incorporates similar elements, but focuses on the implications of inefficient work-at-home policies, taking account of learning-by-doing and heterogeneity across sectors. The last one focuses on optimal mitigation policies of firms in a partial equilibrium setting with stochastic transmission rate, unpredictable vaccine discovery rate and fixed cost of mitigation. The scope of our contribution differs as we explain short run dynamics during the COVID-19 outbreak along with the long run behavior of economic variables in a setting with endogenous stochastic discount factor, unpredictable economic regimes and unpredictable pandemic events.

Section 2 presents the model and provides equilibrium formulas. Section 3 describes the estimation procedure and examines the fit to the data, both long term and during the early stages of the COVID-19 outbreak. Section 4 performs a comparison of models. Conclusions follow. Appendix A details the SEIRD model under a shelter-in-place (SIP) policy. Proofs are in Appendix B. Complementary results are in Appendix C.

2. Economic and Epidemiology Model

We extend the BDRA model in Berrada, Detemple and Rindisbacher (2018) to account for a pandemic outbreak triggered by an unpredictable initial infection event and a subsequent unpredictable vaccine discovery event.

2.1. A Time-Dependent and Stochastic SEIRD Model

The epidemic propagation is assumed to be driven by a SEIRD model with time-dependent infection rate β, unpredictable triggering event and unpredictable vaccination discovery event.

The population is split in five categories: susceptible ($\mathcal{S}$), exposed ($\mathcal{E}$), infectious ($\mathcal{I}$), recovered ($\mathcal{R}$), and deceased ($\mathcal{D}$). Let p_s, p_e, p_i, p_r, p_d be the fractions in each categories, where the sum equals 1. The infectious population further splits in three groups: asymptomatic p_i^{asy}, symptomatic mild p_i^{sm}, and symptomatic severe p_i^{ss}, so that $p_i = p_i^{asy} + p_i^{sm} + p_i^{ss}$. The last two categories consist of mildly sick and severely sick individuals, respectively. We assume $p_i^{ss} = p_i\lambda$, $p_i^{asy} = p_i(1-\lambda)\lambda_w$, $p^{sm} = p_i(1-\lambda)(1-\lambda_w)$ where fractions λ and λ_w are constants. Before the initial infection event, $p_s = 1$ and $p_e = p_i = p_r = 0$. At the initial infection event date τ_0 , the infectious population jumps up and the susceptible population down: $\Delta p_{i\tau_0} > 0$ and $\Delta p_{s\tau_0} = -\Delta p_{i\tau_0} < 0$. Thereafter populations evolve as

$$dp_s = (\mu(1-p_d-p_s) - \beta(t)p_s p_i^{asy} - (\nu^o + \nu 1_{\mathcal{V}_t})p_s)dt \tag{2.1}$$

$$dp_e = (\beta(t)p_s p_i^{asy} - (\mu+\sigma)p_e)dt \tag{2.2}$$

$$dp_i = (\sigma p_e - (\mu + \mu_i + \gamma)p_i)dt \tag{2.3}$$

$$dp_r = (\gamma p_i - \mu p_r + (\nu^o + \nu 1_{\mathcal{V}_t})p_s)dt \tag{2.4}$$

$$dp_d = \mu_i p_i dt \tag{2.5}$$

where the indicator $1_{\mathcal{V}_t}$ indicates a pandemic has occurred and a vaccine has been found. The parameter $\beta(t)$ is the disease transmission rate, a function of time, σ is the incubation rate, γ the recovery rate, ν^o is the natural immunity rate, and ν is the vaccination rate upon discovery of a vaccine. The birth and natural death rates μ are assumed to be equal, hence ensuring a stable population in the absence of disease mortality. Incremental disease mortality is μ_i , and individuals who die as a result of the pandemic are in $\mathcal{D}$. All parameters, except for $\beta(t)$ are constants. The specific form of $\beta(t)$ is described in Section 3.2.1.

A policy intervention such as shelter-in-place (SIP) modifies the dynamics as follows. First, upon implementation, it introduces an outflow at rate q , called the compliance rate, in each of the populations above to corresponding sheltered populations $p_s^Q, p_e^Q, p_i^Q, p_r^Q, p_d^Q$, identified by the superscript Q . Second, upon lifting (LIFT) of the policy, it induces a reverse flow from sheltered populations to those that are not. This reverse compliance rate is q_2 . In the sequel we refer to this model as the SEIRD-SIP-LIFT (SSL) model. Details of the model can be found in Appendix A.

2.2. Regimes, Consumption, Dividends, and Information

We assume there are six regimes: expansion, recession, boom, no pandemic, pandemic and vaccine. The first three regimes are unobservable. They are the outcomes of a Markov chain s_t^m with three states, recession ($s_t^m = e_1$), expansion ($s_t^m = e_2$) or boom ($s_t^m = e_3$), where e_k is the 3×1 -dimensional k^{th} unit vector. The last three are observable and are the outcomes of an independent Markov chain s_t^e with three states, no pandemic ($s_t^e = e_1$), pandemic ($s_t^e = e_2$) or vaccine ($s_t^e = e_3$). The pandemic Markov chain is non-recurrent: it evolves from state e_1 , to e_2 , then e_3 , which is an absorbing state. The vaccine event $1_{\mathcal{V}} = 1$ is triggered when $s_t^e = e_3$. In this event, the dynamics of the susceptible and infectious populations depend on the vaccination rate ν as described in p_s and p_r . To simplify derivations we assume the pandemic is a one-time event, so does not subsequently reoccur: $s_t^e = e_3$ is an absorbing state.

To model the Markov chains, consider independent continuous-time switching process (s^m, s^e)

$$
ds_t^m = \left(\Lambda^m dt + d\tilde{N}_t^m\right)' s_{t-}^m \tag{2.6}
$$

$$
ds_t^e = \left(\Lambda^e dt + d\tilde{N}_t^e\right)' s_{t-}^e \tag{2.7}
$$

where $d\tilde{N}_t^\alpha = dN_t^\alpha - \Lambda^\alpha dt$ for $\alpha \in \{m, e\}$ and N^α is 3×3 -matrix valued Poisson processes with independent off-diagonal elements, diagonal elements $dN_{iit} = -\sum_{j \neq i} dN_{ijt}$, and intensity matrix Λ^α with diagonal elements $\Lambda_{ii}^\alpha = -\sum_{j \neq i} \Lambda_{ij}^\alpha$. Each process takes values $s_t^\alpha \in \{e_i; i = 1, 2, 3\}$ where e_i' denotes the i^{th} unit vector. We can interpret the different states as follows: expansion $s_t^m = e_1$, recession $s_t^m = e_2$, boom $s_t^m = e_3$, no pandemic $s_t^e = e_1$, pandemic $s_t^e = e_2$, pandemic and vaccine $s_t^e = e_3$.[2] A pandemic arises with intensity Λ_{12}^e . As the development of a vaccine takes time $\Lambda_{13}^e = 0$. If there is a pandemic $\Lambda_{21}^e = 0$. The vaccine enters development and becomes available with intensity Λ_{23}^e . Once available the pandemic ends, $\Lambda_{31}^e = \Lambda_{32}^e = 0$. The event triggering the pandemic is determined by the jump of s_t^e to e_2 . The vaccine event resolving the pandemic is determined by the jump to e_3 .

[2] At this stage the labeling of economic regimes is arbitrary. Estimation will show that regime 1 corresponds to a normal expansion regime, 2 to a recession regime and 3 to a boom regime.

The state variables in the model are (C, G, Y) where C is aggregate consumption and (G, Y) are orthogonalized variables constructed from consumption, dividend and unemployment; see Appendix C for details. The model for (C, G, Y) is

$$\frac{dC_t}{C_t} = \left(\mu_o^C(s_t^m) + A^C(s_t^m)F_t^w 1_{\mathcal{E}_t}\right) dt + \sigma^C dW_t^C \tag{2.8}$$

$$\frac{dG_t}{G_t} = \left(\mu_o^G(s_t^m) + A^G(s_t^m)F_t^w 1_{\mathcal{E}_t}\right) dt + \sigma^G dW_t^G \tag{2.9}$$

$$\frac{dY_t}{Y_t} = \left(\mu_o^Y(s_t^m) + A^Y(s_t^m)F_t^w 1_{\mathcal{E}_t}\right) dt + \sigma^Y dW_t^Y \tag{2.10}$$

$$F_t^w = \mu^{p_w^e}(t, s_{t-}^e)/p_{wt}^e \tag{2.11}$$

where F_t^w is a pandemic factor, $A^C(s_t^m), A^G(s_t^m), A^Y(s_t^m)$ are sensitivity parameters capturing the response to the pandemic factor, and $1_{\mathcal{E}_t}$ is the indicator of an epidemic outbreak $\mathcal{E}_t = \{s_t^e \in \{e_2, e_3\}\}$. The pandemic factor is the expected growth rate of the effective workforce p_w^e generated by the SSL model (see end of next section for details), and $\mu_t^{p_w^e}$ is the drift of p_w^e. The processes W^C, W^G, W^Y are independent Brownian motions representing economic shocks. The terms $\left(\mu_o^C(s_t^m), \mu_o^G(s_t^m), \mu_o^Y(s_t^m)\right)$ represent the respective drifts in the absence of an epidemic. The terms involving F_t^w capture the impact of the pandemic on the expected growth rates of (C, G, Y). These components kick in either when an outbreak is in process $s_t^e = e_2$, or when it has already occurred and a vaccine has been found $s_t^e = e_3$. The model (2.8)-(2.10) is a generalization of the reduced form suggested by the pandemic production model in Detemple (2022); it generalizes that specification by allowing for additional state variables (G, Y) and for a dependence on the economic regime s^m.

2.3. Beliefs-Dependent Risk Aversion: BDRA(K,K)

To model economic processes during a pandemic, we extend the BDRA(K,K) model in Berrada, Detemple and Rindisbacher (2018). Let $\mathcal{K} \equiv \{1, ..., K\}$ be a set of regime indices, where K is an arbitrary, but fixed, positive integer. The model has K unobserved economic regimes $s_k^m : k \in \mathcal{K}$, K preference parameters $R_k : k \in \mathcal{K}$ and uses consumption C, orthogonalized dividends G and orthogonalized macro variables Y as information sources. Let $P_k : k \in \mathcal{K}$ be the conditional regime probabilities based on public information. Instantaneous utility of consumption, for population j, is $u_j(c_t,t) = e^{-\beta_u t}\sum_{k=1}^{K} P_{kt} a_j^{R_k} c_t^{1-R_k}/(1-R_k)$ where β_u is a subjective discount rate and $a_j < 1$ is a discount factor depending on the health and employment status of the population. The coefficients R_k are parameters of the risk aversion function, as explained below. Marginal utility of consumption is

$$(2.12) \quad u_{jc}(c_t,t) = e^{-\beta_u t}\sum_{k=1}^{K} P_{kt}\left(\frac{c_t}{a_j}\right)^{-R_k}, \qquad j \in \{s,e,i,r\}$$

and depends on the ratio of consumption to discount factor. Relative risk aversion is $R_{jt}^R = \sum_{k=1}^{K} q_{jkt} R_k$ where $q_{jkt} = \frac{P_{kt} a_j^{R_k} c_t^{-R_k}}{\sum_{k=1}^{K} P_{kt} a_j^{R_k} c_t^{-R_k}}$, different across populations for a given consumption level c_t. As shown in the next section, equilibrium is completely determined by the dynamics of (C,G,Y,P), such that

$$(2.13) \quad dP_{kt} = P_{kt}\left(\mu_{kt}^p dt + \Delta_{kt}^C d\nu_t^C + \Delta_{kt}^G d\nu_t^G + \Delta_{kt}^Y d\nu_t^Y\right)$$

where $\mu_{kt}^p = \sum_{j=1}^{K} P_{jt}\lambda_{jk}/P_{kt}$ with λ_{jk} the transition intensity from regime j to k, and for $\alpha \in \{C,G,Y\}$

$$(2.14) \quad \Delta_{kt}^\alpha = \frac{\mu_k^\alpha - \hat{\mu}_t^\alpha}{\sigma^\alpha}, \qquad d\nu_t^\alpha = \frac{1}{\sigma^\alpha}\left(\frac{d\alpha_t}{\alpha_t} - \hat{\mu}_t^\alpha dt\right), \qquad \frac{d\alpha_t}{\alpha_t} = \mu^\alpha(s_t)dt + \sigma^\alpha dW_t^\alpha$$

$$(2.15) \quad \mu_k^\alpha = \mu^\alpha(s_t^m, s_t^e)_{s_t^m = e_k}; \qquad \mu^\alpha(s_t) = \mu^\alpha(s_t^m, s_t^e) = \mu_o^\alpha(s_t^m) + A^\alpha(s_t^m) F_t^w 1_{\mathcal{E}_t}$$

$$(2.16) \quad \hat{\mu}_t^\alpha = \sum_k \mu_k^\alpha P_k.$$

The processes $\left(\nu^C, \nu^G, \nu^Y\right)$ are informational innovations associated with the underlying Brownian motions, the coefficients $\{\Delta_k^\alpha : \alpha \in \{C,G,Y\}, k \in \mathcal{K}\}$ are sensitivities to news, and $\{\mu_k^p, k \in \mathcal{K}\}$ are the conditional means.

We also assume the supply of labor by households is inelastic. Aggregate labor supply is $\bar{L} = 100$ in the absence of an epidemic. During an outbreak available supply is limited to individuals who do not exhibit symptoms: the workforce is $p_w = p_s + p_e + p_i^{asy} + p_r$. If SIP is implemented, and a fraction h of quarantined individuals is able to work at home, the effective labor supplied is $p_w^e = p_w + \omega p_w^q$ where $\omega < 1$ is an efficiency factor and $p_w^q = p_{s,h}^q + p_{e,h}^q + p_{i,h}^{q,asy} = h\left(p_s^q + p_e^q + p_i^{q,asy}\right)$ is the sheltered population able to work. The effective workforce impacts the growth rate of aggregate variables as described in (2.8)-(2.10).

The model combining the pandemic and economic dynamics described above is called the BDRA-SSL model, which stands for BRDA-SEIRD-SIP-LIFT.

2.4. Equilibrium

The consumption demand of population j is $c_{jt} = a_j I(H_t)$ for a function I commmon to all populations and where $H_t = y\xi_t/a_t$ is the normalized state price density. Aggregate demand is $p_{ct}^a I(H_t)$ where $p_{ct}^a = \sum_{j\in\{s,e,i,r\}} p_{jt}a_j$ is the consumption discount factor of the representative agent.[3] Alternatively, p_{ct}^a can be interpreted as an equivalent population of normal consumers. In equilibrium $p_{ct}^a I(H_t) = C_t$ so that $I(H_t) = C/p_{ct}^a$. The equilibrium allocation satisfies $c_{jt}/a_j = I(H_t) = C_t/p_{ct}^a$, which is identical across populations.

Let $\tau_0 \equiv \inf\{v \geqslant 0 : \Delta N_{12v}^e > 0\}$ be the time marking the birth of the pandemic. At that time the infectious population becomes positive, $\Delta p_{i\tau_0} > 0$, and all quantities related to p_i jump. In particular, the equivalent population of normal consumers jumps from $p_{ct-}^a = a_s = 1$ to $p_{c\tau_0}^a = \sum_{j\in\{s,e,i,r\}} p_{j\tau_0}a_j$.

Equilibrium is then given by

Proposition 2.1. *Consider the BDRA-SSL model and suppose that $t = 0$ is pre-pandemic. The equilibrium stochastic discount factor (SDF), interest rate and market prices of risk are*

$$(2.17) \qquad \xi_t = y\sum_{k=1}^{K} e^{-\beta t}\left(\frac{C_t}{p_{ct}^a}\right)^{-R_k} P_{kt}; \qquad y^{-1} = \sum_{k=1}^{K} C_0^{-R_k} P_{k0}$$

[3]Subgroups of populations can have different discounts for consumption, reflecting their economic status or their health status. The variable p_c^a is adjusted as needed to capture these effects.

$$
\begin{aligned}
(2.18)\qquad r_t =&\beta + \left(\sum_{k=1}^{K} R_k q_{kt}\right)\left(\hat{\mu}_{ot}^C + \left(\widehat{A}_t^C F_t^w - F_t^a\right) 1_{\mathcal{E}_t}\right) - \frac{1}{2}\left(\sum_{k=1}^{K} R_k(1+R_k) q_{kt}\right)(\sigma^C)^2 \\
&- \sum_{k=1}^{K} \mu_{kt}^P q_{kt} + \sum_{k=1}^{K} R_k q_{kt}(\mu_k^C - \hat{\mu}_t^C) + \Lambda_{12}^e \theta_{t-}^J
\end{aligned}
$$

$$
(2.19)\qquad \theta_t^C = \left(\sum_{k=1}^{K} R_k q_{kt}\right)\sigma^C - \sum_{k=1}^{K} q_{kt}\Delta_{kt}^C, \qquad \theta_t^G = -\sum_{k=1}^{K} q_{kt}\Delta_{kt}^G
$$

$$
(2.20)\qquad \theta_t^Y = -\sum_{k=1}^{K} q_{kt}\Delta_{kt}^Y, \qquad \theta_{t-}^J = \sum_{k=1}^{K} \frac{e^{-\beta t}\left(C_t\right)^{-R_k} P_{kt}}{\sum_{k=1}^{K} e^{-\beta t}\left(C_t\right)^{-R_k} P_{kt}}\left(1 - (p_{ct}^a)^{R_k}\right)
$$

where

$$
(2.21)\qquad F_t^w = \frac{\mu^{p_w^e}(t, s_{t-}^e)}{p_{wt}^e}; \qquad F_t^a = \frac{\mu^{p_c^a}(t, s_{t-}^e)}{p_{ct}^a}; \qquad \hat{\mu}_{ot}^C = \sum_k P_{kt}\mu_{ok}^C; \qquad \widehat{A}_t^C = \sum_{k=1}^{K} P_{kt} A_k^C
$$

$$
(2.22)\qquad q_{kt} = \frac{P_{kt}(C_t/p_{ct}^a)^{-R_k}}{\sum_k P_{kt}(C_t/p_{ct}^a)^{-R_k}}.
$$

The quantity $\mu^{p_c^a}(t, s_t^e)$ *is the drift of the aggregate consumption discount factor,* F_t^a *its growth rate,* $\hat{\mu}_{ot}^C$ *is the expected consumption growth rate in the absence of a pandemic,* $\widehat{A}_t^C = \sum_{k=1}^{K} P_{kt} A_k^C$ *is the expected value of* $A^C(s^m)$ *,* q_{kt} *is the equilibrium pricing measure, and* θ_{t-}^J *is the market price of jump risk. The interest rate has a jump component* $\theta_{t-}^J \Lambda_{12}$ *.*

Remark 2.2. *The SDF is marginal utility evaluated at the equilibrium consumption allocation. Note that it is discontinuous: it jumps down at* τ_0 *, and the relative jump size, i.e., the negative of the market price of jump risk, is*

$$
(2.23)\qquad \frac{\Delta \xi_{\tau_0}}{\xi_{\tau_0 -}} = \frac{\sum_{k=1}^{K} C_{\tau_0}^{-R_k} P_{k\tau_0}\left(\left(p_{c\tau_0}^a\right)^{R_k} - 1\right)}{\sum_{k=1}^{K} C_{\tau_0}^{-R_k} P_{k\tau_0}} < 0.
$$

where $p_{c\tau_0}^a = 1 + \Delta_i(\lambda_i + \lambda_s a_i - 1)$ *and* Δ_i *is the size of the jump in* p_i *at* τ_0 *. Coefficient* $\lambda_s = (1-\lambda)(1-\lambda_w)$ *is the fraction of symptomatic mild in the infectious population, while*

$\lambda_i = (1-\lambda)\lambda_w$ *is the fraction of asymptomatic. The expected relative jump is*

$$(2.24)\quad E_{\tau_0-}\left[\frac{\Delta\xi_{\tau_0}}{\xi_{\tau_0-}}\right] = \frac{\sum_{k=1}^{K} C_{\tau_0}^{-R_k} P_{k\tau_0}\left(\left(p_{c\tau_0}^a\right)^{R_k} - 1\right)}{\sum_{k=1}^{K} C_{\tau_0}^{-R_k} P_{k\tau_0}} \Lambda_{12}^e dt < 0.$$

The epidemic impact on the structure of the SDF is through p_{ct}^a, the equivalent population of normal consumers. A decrease in p_{ct}^a increases consumption per head, hence reduces the SDF. There are three effects on equilibrium coefficients. The first, encapsulated in the term $\hat{A}_t^C F_t^w - F_t^a$, is structural in nature. It represents the net impact on the expected output growth rate and the growth rate of the equivalent population of normal consumers. The second, arises through the adjusted probabilities q_{kt} which depend on $c_{jt}/a_j = C_t/p_{ct}^a$. The third arises through the jump associated with the initial infection event. Variations in the equivalent consuming population p_{ct}^a combine with variations in consumption and regime probabilities to determine the behavior of these effects over time. The interest rate level and evolution reflect all effects. Market prices of risk reflect the second and third effects.

The next proposition extends the stock valuation formula in Berrada, Detemple and Rindisbacher (2018) to the epidemic context.

Proposition 2.3. *Define the matrix* $\Upsilon(t, s_t^e)$ *as in Proposition 6.1 in the Appendix and suppose that its elements* $\Upsilon_{ij}(t, s_t^e)$ *are finite for all pairs* (i,j). *The stock price is then given by*

$$(2.25)\quad S_t = \mathsf{E}_t\left[\int_t^\infty \xi_{t,s} D_s ds\right] = D_t Z_t' \Upsilon(t, s_t^e) P_t$$

where $\mathsf{E}_t[\cdot]$ *is the conditional expectation operator and* $Z_t = [..., q_{kt}/P_{kt}, ...]'$ *is the density of the probability measure* q *with respect to* P. *The stock market return volatility is* $\sigma_t^S = \sqrt{(\sigma_t^{SC})^2 + (\sigma_t^{SG})^2 + (\sigma_t^{SY})^2}$ *where*

$$(2.26)\quad \begin{bmatrix} \sigma_t^{SC} \\ \sigma_t^{SG} \\ \sigma_t^{SY} \end{bmatrix} = \begin{bmatrix} \rho\sigma^D + \sigma_t^{SCR} + \sigma_t^{SCG} \\ \sqrt{1-\rho^2}\sigma^D + \sigma_t^{SGG} \\ \sigma_t^{SYG} \end{bmatrix}$$

and, using $diag_K(v)$ for the diagonal $K \times K$ matrix with vector v on the diagonal,

$$\sigma_t^{SCR} = Z_t' diag_K[-R_k \sigma^C] \left(\frac{\Upsilon(t, s_{t-}^e)}{Z_t' \Upsilon(t, s_{t-}^e) p_t} - I_K \right) P_t, \tag{2.27}$$

$$\sigma_t^{S\alpha G} = Z_t' \left(\frac{\Upsilon(t, s_{t-}^e)}{Z_t' \Upsilon(t, s_{t-}^e) P_t} - I_K \right) \text{diag}\left[\Delta_{kt}^{\alpha}\right] P_t, \qquad \alpha \in \{C, G, Y\}. \tag{2.28}$$

The component σ_t^{SCR} is the volatility of Z_t due to consumption uncertainty, and the components $\sigma_t^{SCG}, \sigma_t^{SGG}, \sigma_t^{SYG}$ are associated with beliefs uncertainty. The correlation between the stock return and the consumption growth rate (resp. orthogonalized dividend growth rate) is $\rho_t^{SC} = \sigma_t^{SC}/\sigma_t^S$ (resp. $\rho_t^{SD} = \sigma_t^{SD}/\sigma_t^S$). Correlations are stochastic.

Remark 2.4. *Note that the equilibrium stock price and its volatility coefficients are continuous. In contrast, the state price density is discontinuous, because marginal utility jumps at the pandemic starting time. Market prices of diffusion risk are independent of the pandemic state variable s_t^e , hence are continuous. The market price of jump risk is discontinuous. The equity premium, as the product of market prices of diffusion risk and volatility components, is continuous as well.*

Remark 2.5. *The stock price has the decomposition $S_t = S_t^{np} + S_t^p$ where $S_t^{np} = D_t Z_t' \overline{\Upsilon} P_t$ and $S_t^p = D_t Z_t' \left(\Upsilon(t, s_t^e) - \overline{\Upsilon}\right) P_t$ represent, respectively, the price when a pandemic cannot arise and when a pandemic is possible. The matrix $\overline{\Upsilon}$ is defined in (6.6).*

3. Empirical Results

We proceed in two stages. First we estimate the model without pandemic effects, based on pre-pandemic data. Second, we estimate pandemic-related parameters, using data during the COVID-19 outbreak.

3.1. Estimating the BDRA Model: Before the Pandemic

The estimation for the BDRA(K,K) model without pandemic effects follows the approach in BDR (2018). Estimation is based on longer time series with 5 additional years of data.

3.1.1. Data Description

The estimation is based on quarterly data from January 1957 to December 2019. The per capita consumptions of nondurable goods ($C_{n,t}$) and services ($C_{s,t}$) are obtained from the Saint-Louis Federal Reserve Bank. Consumption growth is defined as

$$\ln \frac{C_{s,t+1} + C_{n,t+1}}{C_{s,t} + C_{n,t}}, \tag{3.1}$$

Other time series are constructed as in Beeler and Campbell (2012). Using the CRSP value weighted return indexes including dividends (vwretd_t) and excluding dividends (vwretx_t) gives the dividend series D_t ,

$$P_{t+1} = P_t \left(1 + \mathrm{vwretx}_{t+1}\right), \qquad D_{t+1} = P_{t+1} \left[\frac{1 + \mathrm{vwretd}_{t+1}}{1 + \mathrm{vwretx}_{t+1}} - 1 \right]. \tag{3.2}$$

The price-dividend ratio (PDR) is obtained by dividing the current price index level by the sum of the 12 previous months' dividends. All further computations and estimations use the log of the PDR. Quarterly returns are constructed from log monthly returns. Real returns are obtained by adjusting for inflation using the seasonally adjusted consumer price index (obtained from the Saint-Louis Federal Reserve Bank). Quarterly series of ex-ante real three-month rates and real ten-year rates are constructed from monthly series of nominal yields as in Beeler and Campbell (2012). The ex-post real rate is obtained by subtracting the realized inflation from the observed three-month treasury bill rate. It is then regressed against the average quarterly log inflation over the previous year $\pi_{t-12,t}$ (annual log inflation divided by four) and the three-month nominal yield $y_{3,t}$,

$$y_{3,t} - \pi_{t,t+3} = \beta_0 + \beta_1 y_{3,t} + \beta_2 \pi_{t-12,t} + \varepsilon_{t+3}. \tag{3.3}$$

The ex-ante real rate is then defined as $\hat{\beta}_0 + \hat{\beta}_1 y_{3,t} + \hat{\beta}_2 \pi_{t-12,t}$. The same procedure is used, with an adjustment for the time period, for the ten-year ex-ante real rate.[4]

The information variable in Eq. (2.10) is defined as the unemployment rate (UE), $I_t = UE_t$. The data for UE is obtained from the Saint-Louis Federal Reserve Bank.

3.1.2. Estimation Procedure

Model parameters are estimated using a just identified sequential GMM procedure pioneered by Ogaki (1993). The set of parameters is partitioned into subsets $\Theta = \Theta_1 \cup \Theta_2 \cup \Theta_3$ with

$$\begin{aligned}
&\Theta_1 \equiv \left\{\sigma^C, \sigma^D, \sigma^I, \rho, \rho^{IC}, \rho^{ID}\right\}, \qquad \Theta_3 \equiv \{R_2, R_3\} \\
&\Theta_2 \equiv \left\{\mu_1^C, \mu_2^C, \mu_3^C, \mu_1^D, \mu_2^D, \mu_3^D, \mu_1^I, \mu_2^I, \mu_3^I, \lambda_{12}, \lambda_{13}, \lambda_{21}, \lambda_{23}, \lambda_{31}, \lambda_{32}, R_{\min}, \beta\right\}.
\end{aligned}$$

The first subset, Θ_1 , contains parameters of the covariance matrix of consumption, dividends and the information variable (unemployment). Parameter estimates are obtained by matching corresponding sample moments. Given the constant volatility structure of state variables these estimates are equivalent to maximum likelihood estimates (MLE).

The second subset, Θ_2 , determines the steady state behavior of the model. These parameters are estimated using sample analogs of the invariant theoretical counterparts.

Parameters in the third subset, Θ_3 , do not affect the steady state equilibrium values, but only the dynamics of equilibrium quantities. In order to address this part of the estimation procedure, we rely on the extensive literature originating from Campbell and Shiller (1988) that identifies a link between stock returns and PDR. We consider the following two moment conditions (i) correlation between log simple returns and changes in log PDR, and (ii) correlation

[4] This procedure is also used by Harvey (1988) to test whether the real term premium can forecast recessions.

between log simple returns and changes in log PDR lagged by one quarter. Given the estimates for parameters in the subset $\Theta_1 \cup \Theta_2$, these two moments within the model use filtered values of state variables to generate a sample path that depends on the unknown parameters in Θ_3. Parameters in Θ_3 are estimated by minimizing the squared error of deviations of these two moments of sample paths within the model and in the statistical sample.

Table 1 summarizes the moment conditions used in the estimation of the different sets of parameters. Additional details and justification of this procedure can be found in BDR (2018).

3.1.3. Parameter Estimates and Model Performance

Table 2 shows that parameter estimates are close to their empirical values, and typically lie within the 95% confidence bands or are close to the edges of these bands. Exceptions are the mean 3-month and 10-year yields and the volatility of the 10-year yield. Relative to the estimation results in BDR (2018), which is based on the shorter sample from 1957 to 2014, the mean consumption growth rate is further away from its sample value.

Table 3 reports estimates for the drifts of consumption, unemployment, and dividends, and for the preference parameters, in the three growth regimes. Patterns for the coefficients pertaining to consumption and unemployment are the same as in BDR (2018), with reduction in some of the point values obtained. In contrast, dividend drift coefficients display an increasing pattern, as opposed to the previous U-shape pattern, due to an increase in the estimate for regime 2. The risk aversion function implied by estimates of preference parameters displays the same inverted U-shape as in BDR (2018), but with a slight upward shift. Taken together, these results suggest the interpretation of regime 2 as a recession regime is also maintained, even though neither estimation imposed a priori restrictions on the ordering of regimes. Finally, standard deviation estimates for consumption, dividend and unemployment are about the same, whereas the correlations between dividend and consumption (positive), and dividend and unemployment (negative) are both cut in half.

Overall, the results obtained based on the augmented sample 1957-2019 are consistent with those in BDR (2018) for the period 1957-2014.

Table 1: Moment conditions. The table lists the moment conditions used for the just identified sequential GMM estimation of model parameters. Theoretical expressions for steady state values are in Detemple et al (2018). Sample moments are based on standard sample statistics for means, standard deviations, correlation, and auto-correlation coefficients. The operator $\widehat{CORR}_{T,\Theta_3}[X_t, Y_t]$ calculates the empirical correlation coefficient between X_t and Y_t based on model trajectories of length T as a function of parameters Θ_3 .

Parameter estimation: moment conditions		
Moment condition	Invariant moment (definition)	Sample moments
Covariance of state variables: $\Theta_1 = \left\{\sigma^C, \sigma^D, \sigma^I, \rho, \rho^{IC}, \rho^{ID}\right\}$		
1. Vol. cons.	σ^C	$\widehat{STD}_T[\Delta \log C_t]$
2. Vol. div.	σ^D	$\widehat{STD}_T[\Delta \log D_t]$
3. Vol. unemp.	σ^I	$\widehat{STD}_T[\Delta \log I_t]$
4. Corr. cons., div.	ρ	$\widehat{CORR}_T[\Delta \log C_t, \Delta \log D_t]$
5. Corr. cons., unemp.	ρ^{IC}	$\widehat{CORR}_T[\Delta \log C_t, \Delta \log I_t]$
6. Corr. div., unemp.	ρ^{ID}	$\widehat{CORR}_T[\Delta \log D_t, \Delta \log I_t]$
Steady state values: $\Theta_2 = \left\{\mu_1^C, \mu_2^C, \mu_3^C, \mu_1^D, \mu_2^D, \mu_3^D, \mu_1^I, \mu_2^I, \mu_3^I, \lambda_{12}, \lambda_{13}, \lambda_{21}, \lambda_{23}, \lambda_{31}, \lambda_{32}, R_{\min}, \beta\right\}$		
1. Exp. cons.	$\mu_\infty^C + 0.5\left(\sigma^C\right)^2$	$\hat{E}_T[\Delta \log C_t]$
2. Exp. div.	$\mu_\infty^D + 0.5\left(\sigma^D\right)^2$	$\hat{E}_T[\Delta \log D_t]$
3. Exp. unemp.	$\mu_\infty^I + 0.5\left(\sigma^I\right)^2$	$\hat{E}_T[\Delta \log I_t]$
4. Log-PDR	$\log \frac{S_\infty}{D_\infty}$	$\hat{E}_T[\log PDR_t]$
5. Exp. 3-m. yield	$Y_\infty^{\infty+0.25}$ $\tau = 0.25$	$\hat{E}_T\left[Y_t^{t+0.25}\right]$
6. Exp. 10-y. yield	$Y_\infty^{\infty+10}$ $\tau = 10$	$\hat{E}_T\left[Y_t^{t+10}\right]$
7. Stock volatility	σ_∞^S	$\widehat{STD}[\Delta \log S_t]$
8. Volatility of 10-y. yield	$\sigma_\infty^Y(\tau)$	$\hat{E}_T\left[Y_t^{t+0.25}\right]$
9. Exp. excess return	$\mu_\infty^S - r_\infty$	$\hat{E}_T[\Delta \log S_t - r_t]$
10. Corr. return, cons.	$\rho_\infty^{S,C}$	$\widehat{CORR}_T[\Delta \log S_t, \Delta \log C_t]$
11. Corr. return, div.	$\rho_\infty^{S,D}$	$\widehat{CORR}_T[\Delta \log S_t, \Delta \log D_t]$
12. Corr. 3-m. yield, cons.	$\rho_\infty^{Y,C}(\tau)$ $\tau = 0.25$	$\widehat{CORR}_T\left[Y_t^{t+0.25}, \Delta \log C_t\right]$
13. Corr. 3-m. yield, div.	$\rho_\infty^{Y,D}(\tau)$ $\tau = 0.25$	$\widehat{CORR}_T\left[Y_t^{t+0.25}, \Delta \log D_t\right]$
14. Corr. 10-y. yield, cons.	$\rho_\infty^{Y,C}(\tau)$ $\tau = 10$	$\widehat{CORR}_T\left[Y_t^{t+10}, \Delta \log C_t\right]$
15. Corr. 10-y. yield, div.	$\rho_\infty^{Y,D}(\tau)$ $\tau = 10$	$\widehat{CORR}_T\left[Y_t^{t+10}, \Delta \log D_t\right]$
16. Volatility log-PDR ratio	$\sigma_\infty^{\log-\mathrm{PDR}}$	$\widehat{STD}_T[\log PDR_t]$
17. Corr. log-PDR, cons.	$\rho_\infty^{\log-\mathrm{PDR},C}$	$\widehat{CORR}_T[\log PDR_t, \Delta \log C_t]$
Path dynamics: $\Theta_3 = \{R_2, R_3\}$		
1. Corr. log-PDR, return	$\widehat{CORR}_{T,\Theta_3}[\Delta \log \mathrm{PDR}_t, \Delta log S_t]$	$\widehat{CORR}_T[\Delta \log \mathrm{PDR}_t, \Delta log S_t]$
2. Corr. log-PDR, return (1 lag)	$\widehat{CORR}_{T,\Theta_3}[\Delta \log \mathrm{PDR}_{t-1}, \Delta log S_t]$	$\widehat{CORR}_T[\Delta \log \mathrm{PDR}_{t-1}, \Delta log S_t]$

Table 2: Moment conditions and confidence intervals. Model moment conditions are based on stationary values and estimated parameters. Confidence bounds are obtained using the stationary bootstrap for weakly dependent data of Politis and Romano (1994). The 95% confidence intervals are based on 1000 replications and optimal average blocksize.

	Model	Data	Confidence lower bound	Confidence upper bound
Mean				
Consumption growth	0.01336	0.01878	0.01619	0.02094
Dividend growth	0.00862	0.02089	0.00842	0.03150
Unemployment growth	0.00586	0.00492	-0.03042	0.02911
Log PDR	3.77885	3.61139	3.56689	3.66143
Excess returns	0.05318	0.05238	0.00914	0.09553
Mean 10-year yield	0.02919	0.02187	0.02083	0.02299
Mean 3-month yield	0.02968	0.00864	0.00691	0.01048
Volatility				
Log PDR	0.16681	0.17046	0.15448	0.19169
Excess returns	0.21168	0.16792	0.14972	0.19018
10-year yield	0.02101	0.00902	0.00828	0.01004
Correlations				
Stock returns / consumption	0.08920	0.24046	0.11367	0.36834
Stock returns / dividend	0.26655	0.09437	–0.04243	0.20755
10-year yield / consumption	0.12260	0.14894	0.00985	0.27520
10-year yield / dividend	-0.04092	-0.17219	-0.27332	-0.06401
3-month yield / consumption	0.26685	0.25407	0.13769	0.36103
3-month yield / dividend	-0.02821	-0.08680	-0.20495	0.04073
log PDR / consumption	0.26323	0.22340	0.08522	0.35540
Stock return and log(PDR) correlation				
Contemporaneous	0.99716	0.96457	0.9402	0.9758
Lagged log(PDR)	0.06060	0.06030	-0.0707	0.2064

Table 3: Estimated parameters (standard errors). GMM parameter estimates with standard errors obtained from stationary bootstrap (Politis and Romano (1994)).

Growth regime			Growth regime		
Normal	Low	High	Normal	Low	High
Consumption			Unemployment		
μ_1^C	μ_2^C	μ_3^C	μ_1^{UE}	μ_2^{UE}	μ_3^{UE}
0.00969	0.00572	0.03554	-0.00067	0.12653	–0.09982
(0.0081)	(0.0075)	(0.0102)	(0.0332)	(0.0460)	(0.0424)
Dividend			Preferences: risk aversion		
μ_1^D	μ_2^D	μ_3^D	R_1	R_2	R_3
0.00672	0.00746	0.01707	2.06340	2.5550	2.2416
(0.0099)	(0.0098)	(0.0104)	(0.3788)	(0.0983)	(0.0133)

Preferences: subjective discount rate		
β_1	β_2	β_3
0.01000	0.01000	0.01000
(0.0021)	(0.0021)	(0.0021)

Standard deviations and correlations

	Consumption	Dividend	Unemployment
Consumption	0.0092	0.0799	–0.3626
	(0.0641)	(0.1096)	(0.2230)
Dividend	0.0799	0.0449	–0.1836
	(0.1096)	(0.0744)	(0.1895)
Unemployment	–0.3626	–0.1836	0.1214
	(0.2230)	(0.1895)	(0.9587)

Infinitesimal generator (intensity matrix)

	Normal	Low	High	Steady state probabilities
Normal	–0.07343	0.07343	3.859425 E-07	0.645
	-	(0.0148)	(1.86 E-06)	
Low	0.24417	–0.25736	0.01320	0.184
	(0.0343)	-	(0.0037)	
High	0.01426	1.789710 E-07	–0.01426	0.170
	(0.0046222)	(1.70 E-06)	-	

3.2. Estimating the BDRA Model: During the Pandemic

We now focus on the pandemic period, assuming that parameters $A^C(s_t^m) = A^C, A^G(s_t^m) = A^G$ are constant across economic regimes. First, we complete the SSL model by specifying the transmission intensity. Second, we describe the estimation procedure for the pandemic-related parameters. Last, we present the results and discuss performance.

3.2.1. Transmission Intensity Specification

We consider a version of the SSL pandemic model with time-decay and threshold effects in the transmission intensity β. We assume

$$\beta_t = \beta_0 e^{-\kappa_0 t} 1_{t \leqslant t_1} + \beta_1 e^{\kappa_1 (t - t_m)} 1_{t_1 < t \leqslant t_2} + \beta_2 e^{-\kappa_2 (t - t_2)} 1_{t_2 < t} \tag{3.4}$$

where t_1, t_2 are transmission intensity change dates, κ_0, κ_2 are decay rates respectively prevailing up to the first date and after the second one, and κ_1 is an decay/expansion rate in the intermediate period up to time t_2. The parameter $\beta_1 = \beta_0 e^{-\kappa_0 t_1}$ is the value at t_1 and $\beta_2 = \beta_1 e^{\kappa_1 (t_2 - t_m)}$ at t_2. The parameter $t_m \in [t_1, t_2]$ cuts the intermediate period in two parts. From t_1 to t_m the transmission intensity decreases, from t_m to t_2 it increases, hence the dual interpretation of κ_1. This formulation captures social distancing effects taking place as the epidemic propagates and disease mitigation recommendations by health authorities and governmental agencies. For instance, the dates t_1, t_2 might be associated with recommendations to implement and lift a SIP policy. The reversal of decay during the period $[t_1, t_2]$ captures weariness and overconfidence effects that may develop during SIP.

3.2.2. Estimation Procedure for Pandemic Parameters

In light of Sections 2.1 and 3.2.1, and Appendix A, the set of pandemic propagation parameters is $\Theta_4 = \{\beta_0, t_0, t_1, t_2, t_m, \kappa_0, \kappa_1, \kappa_2, \sigma, \gamma, \mu_i, \mu, \nu^o, \lambda, \lambda_w, q, q_2\}$.[5] In addition, we have parameters

[5] We estimate a version of the model with $\nu = 0$.

in $\Theta_5 = \{A^C, A^D, A^U(s_t^m), a_i, a_l, \omega, h\}$ governing the impact of the pandemic on the time series of consumption, dividend and unemployment. Hence, the full set of pandemic-related parameters to be estimated is $\Theta_4 \cup \Theta_5$.

Estimation is based on the number of new COVID-19 cases, the level of the S&P 500 index during the outbreak and a measure of the index return volatility. Data for new cases are from the COVID Tracking Project.[6] Volatility is proxied by the average squared total return on the S&P 500 index computed over a 10 days rolling window. The sample period is January 1, 2020 until August 7, 2020, therefore covering the first and second waves of the COVID pandemic in the US.[7]

All target quantities are available at daily frequency. Input quantities in the model, however, are available at different frequencies. Unemployment, consumption and dividend are available at monthly frequency and are held constant between observations. This results in innovation processes that are updated at monthly frequency. The regimes conditional probabilities P_t therefore change at monthly frequency. The drift processes of unemployment, consumption and dividend, are adjusted at daily frequency using the pandemic related effect $A_t^\alpha(s_t^m)F_t^w 1_\mathcal{E}$. The stock price level and volatility are functions of the conditional probabilities, the consumption and dividend level. They also depend on the volatility of the conditional probabilities which are functions of the drift processes of unemployment, consumption and dividend. It follows that through the updating procedure of the drift processes driven by the pandemic model, stock price level and volatility can also be updated at daily frequency. The entire process is displayed in a diagram in Figure 1. The estimation is performed jointly by minimizing the weighted squared distance between model implied and observed (i) stock volatility (ii) stock price level and (iii) number of new COVID cases, all measured at daily frequency. The weights applied ensure that time series have the same average.[8] Joint estimation of parameters in $\Theta_4 \cup \Theta_5$ is

[6]See https://covidtracking.com/data/us-daily

[7]The quantitative easing program started in March 2020 with a significant inflation of the FED balance sheet. There is strong empirical evidence that QE affected stock prices, but with a significant delay. We focus on the immediate real effect of the pandemic and do not extend the analysis to a period where the market is too heavily biased by QE.

[8]The reference average is arbitrary. We use the average volatility in our implementation. Thus, we adjust

justified by the fact that populations behavior affects the pandemic propagation parameters, in particular the infection rate (3.4) and its evolution through time.

3.2.3. Parameter Estimates

The lower panel in Table 4 reports estimates of pandemic propagation and related policy parameters in Θ_4. The initial transmission rate $\beta_0 = 2.345420$ is found to decay at rate $\kappa_0 = 3.625968$ pre-SIP, decay/appreciate at rate $\kappa_1 = 22.887898$ during SIP, to finally decay at rate $\kappa_2 = 12.877192$ post-SIP. Estimates of infection regime changes are respectively $t_1 = 61.031222$ (days) and $t_2 = 123.08807$ (days), roughly in line with average times of SIP and LIFT implementations across states. The pandemic birth time is estimated at $\tau_0 = 12.287299$ (days), and the time marking an acceleration of transmission during SIP is $t_m = 64.078406$ (days). The mean latency duration is $\sigma^{-1} = 15.665977$ days, and the mean infectious duration $\gamma^{-1} = 12.540573$ days. Both values are consistent with estimates reported during the initial phases of the COVID-19 outbreak. The fraction of severe and asymptomatic cases are estimated at $\lambda = 0.018777$ and $(1-\lambda)\lambda_w = 0.622215$, respectively, again consistent with reported values. The disease mortality parameter $\mu_i = 2.22 \times 10^{-5}$ is commensurate with COVID-19 mortality statistics. As might be expected, the natural immunity rate $\nu^o = 1,2489 \times 10^{-5}$ is extremely low. Finally, the migration rates into and out of lockdown are respectively $q = 0.080264$ and $q_2 = 0.000620$. Compliance q is low because some states never went into lockdown while others implemented SIP at various dates. In addition, the policy did not apply to essential workers. Reverse migration q_2 is even lower because businesses were slow to reopen or because firms continued operating using work-at-home.

time series F_i as $F_{ij}^{adjusted} = F_{ij} \times (\bar{V}^{data}/\bar{F}_i^{data})$ where $\bar{V}^{data}$ is the mean volatility over the sample period, $\bar{F}_i^{data}$ is the mean of F_i^{data} and the subscript j denotes the sampling time $t_j : j = 1, ..., N_j$.

Table 4: Estimated coeficients for the BDRA-SSL model. Sample period for estimation is January 1, 2020 to August 7, 2020.

Economic Model

Parameters	Estimate
$A^U(s_t^m = e_1)$	-0.025679074
$A^U(s_t^m = e_2)$	-0.000101566
$A^U(s_t^m = e_3)$	-0.466881675
$A^C(s_t^m)$	0.000465526
$A^D(s_t^m)$	0.001137158
a_i	0.99979819
a_l	0.999967397
ω	0.04120106
h	0.999786164

Pandemic Model

Parameters	Estimate
β_S	2.345420310
σ	0.063832594
γ	0.079741168
λ	0.018777052
λ_w	0.634122452
μ_i	0.000005600
ν^o	1.24892E-05
μ	0.000022200
κ_0 (pre SIP)	3.625968997
q	0.080264840
q_2	0.000620225
κ_1 (during SIP)	22.88789899
κ_2 (post SIP)	12.87719289
t_1	61.03122276
t_2	123.08807000
t_m	64.07840632
τ_0 (pre SIP)	12.28729912

The upper panel of Table 4 reports estimates of the economic effects of the pandemic on the drifts of consumption, orthogonal dividend and orthogonal unemployment. The sensitivity of consumption, assumed to be constant across economic regimes, is estimated at $A^C = 0.000465$, showing a low response to the propagation via p_w^e . The sensitivity of dividend, also assumed constant, is higher at $A^D = 0.001137$. Estimates of both of these coefficients are positive indicating a negative impact as the growth rate of the effective workforce falls. In contrast the sensitivity of orthogonal unemployment, assumed to depend on the economic regime in the estimation, is negative in all of these regimes. Its greatest magnitudes are in regimes $s_t^m = e_1$ and $s_t^m = e_3$ at respectively $A^U(e_1) = -0.025679$ and $A^U(e_3) = -0.466881$. Unemployment responds strongly to the growth rate of the workforce if the economy is in a normal or boom regime when the pandemic takes of. At $A^U(e_2) = -0.000101$, the response during a downturn is much weaker. Uncertainty about the regime implies that the actual response of unemployment is determined by the average of these sensitivities, which is unambiguously negative. A negative expected growth in the effective workforce therefore translates into an expected increase in unemployment, and that response becomes stronger if regime probabilities shift towards the normal and boom regimes as the pandemic unfolds. The efficiency of work-at-home is estimated at a low $\omega = 0.041201$, and the fraction of individuals working at home is $h = 999786$. The efficiency loss associated with work-at-home can be attributed to frictions in the organization of work, the transmission of information and the implementation of decisions and processes. Last, the consumption discount factors of ill and laid-off individuals are estimated at $a_i = 0.999798$ and $a_l = 0.999967$, respectively. Individuals stricken by the pandemic shift their consumption basket towards medical goods and services, leading to a very small reduction in overall expenditures. Laid-off individuals consume at nearly the same rate during the pandemic due to government subsidies and related support schemes.

3.2.4. Model Performance: Targeted Variables

We now examine the performance of the BDRA-SSL model relative to variables that were targeted in the estimation procedure, i.e., the number of new COVID-19 cases, the volatility of the S&P 500, and the level of the S&P 500.

Figure 2 shows that the estimated model stays close to the observed number of cases in the data and picks up the timing of changes in the propagation pattern. The most significant deviation occurs toward the end of the first wave of the outbreak, between days 130 and 150 counting from January 1, 2020. The match during the second wave, between days 160 and 220, is very close.

Figure 3 demonstrates that the BDRA-SSL model is able to replicate the rapid increase and decrease in volatility that took place during the first wave of the COVID-19 pandemic as well as the magnitude and inverted V-shape of the effect recorded, i.e., the volatility spike. In comparison the standard BDRA model without pandemic effect, called the base model hereafter, only generates an increase in volatility with a significant delay, and of much smaller amplitude; see Figure 7. It is also unable to reproduce the spike of the volatility event. The reason for the discrepancy between the performances of the two models is because the base model reacts only when the recession probability reaches a peak, whereas the pandemic model reacts immediately following an increase in the number of COVID-19 cases. This discrepancy is examined in more details in Section 3.2.5 below.

Figure 4 establishes that the BDRA-SSL model is able to reproduce the behavior of the S&P 500 during the first two waves of the outbreak. The model generates the asymmetric V-shape adjustment of the index and nearly matches the timing of the trough. It also matches the steep decline of the index along with some of its temporary fluctuations, albeit with an overshoot prior to the decline. Finally, it displays the progressive recovery found in the data, but with more pronounced short term swings.

3.2.5. Regime Probabilities and Pandemic Model

To better understand the performance of BDRA-SSL, it is informative to focus on the dynamics of the conditional regime probabilities. Figure 5 and 6 display their evolution for the model with pandemic (BDRA-SSL) and the base model (BDRA). The shaded area corresponds to the brief recession period February through April identified by NBER. The base model overestimates the duration of the recession, and has a major reaction with a delay of two months. The volatility in the base model, illustrated in Figure 7, increases with a delay exceeding two months and stays high for several months thereafter. It therefore completely misses the observed spike in volatility during the first wave of the pandemic. In contrast, the conditional probabilities in BDRA-SSL react sooner and with smaller magnitudes; see Figure 5. The increase in the recession probability is confined to the NBER recession period, and it goes to zero immediately when this recession is assessed to be over. Symmetrically, the normal regime probability decreases during the NBER-declared recession, but rapidly goes to one thereafter. The volatility implied by BDRA-SSL is directly impacted by the variations in the number of COVID cases through the pandemic factor F_t^w, hence through changes in the expected drifts of consumption, unemployment and dividends, and through associated changes in the regime probabilities. The model's ability to rapidly reflect short term variations tied to the epidemic not only generates a high level of volatility at the onset of the crisis, but is also able to capture its rapid decrease as the number of new cases decreases. The introduction of this pandemic channel in BDRA-SSL allows it to correctly estimate the duration of the recession, perfectly time the spike in volatility, and match the magnitude and profile of the volatility event.

Figure 3 shows there is a second volatility event in the data, very short-lived and of small magnitude, between days 160 and 170 of the sample. This event is not picked up by BDRA-SSL even though the pandemic flares again during the second wave, roughly between days 160 and 220 in the sample. As indicated above the recession (normal regime) probability is null (one) during that period, implying the model becomes very responsive to pandemic shocks. The reason why volatility does not spike in the model is because the pandemic factor F_t^w is close to null, i.e., p_w^e is nearly flat, during that period, implying the absence of a significant reaction in the underlying factors and the regime probabilities (see Figure 8).

4. Comparison of Models

We now compare the performances of different models with BDRA-SSL. Contenders are the nested alternatives, CRRA-SSL, BDRA and BDRA-SSL-C, and the non-nested BDRA-SIRD-SL model. The model CRRA-SSL has constant parameters $R_k = R : k \in \mathcal{K}$ across regimes.

In BDRA, the econonic model does not depend on the SSL component: $A^C = A^D = A^U = a_i = a_l = 0$ and $\omega = h = 1$. BDRA-SSL-C has constraints $\omega \geqslant 0.7, h \geqslant 0.9$ on efficiency and work-at-home fraction. The non-nested BDRA-SIRD-SL model has SIRD pandemic dynamics instead of SEIRD. In this specification, contaminated individuals transition directly from the susceptible category to the infectious category. The remainder of the model, in particular the policy components, SIP (S) and LIFT (L), remain the same. All models are estimated using the sequential procedure described in previous sections. Parameter estimates are in Table 5. As expected, estimates of pandemic parameters, which are jointly estimated, display small variations across models, reflecting structural changes in models, including behavioral feedback effects.

Parameters of the pandemic model are estimated using a quasi-log-likelihood ratio (QLR) estimator. Let F_{ij} denote time series F_i at sampling times $t_j : j = 1, ..., N$. BDRA-SSL-C, CRRA-SSL, and BDRA, are all nested in BDRA-SSL. The QLR estimator minimizes the sum of squared errors over multiple time series

$$(4.1) \qquad J_N \equiv SSE(N, Q) = \sum_{i,j}^{N,Q} \left(F_{ij}^{data} - F_{ij}^{model}\right)^2$$

where N is the number of time points, and Q the number of time series involved. It can be computed over targeted variables $Q = 3$ or subsets thereof $Q < 3$, and measures the fit of the model to the data. Table 6 provides test results based on number of cases, stock volatility, and the stock price in the the sample and in the model. The BDRA-SIRD-SL model is not nested. To assess its relative performance Bayesian and Akaike information criteria are calculated.

Table 6 shows that model specification tests reject the hypothesis that any of the nested alternatives, BDRA-SSL-C, CRRA-SSL, and BDRA, dominates BRDRA-SSL. This is confirmed by both BIC and AIC model selection criteria. The table also shows that the non-nested BDRA-SIRD-SL model is dominated. Both the BIC and AIC model selection critera choose BDRA-SSL as the best model among all alternative specifications, nested and non-nested, despite it being least parsimonious.

Table 5: Estimated coeficients for BDRA-SSL, CRRA-SSL, BDRA and BDRA-SSL-C (constrained). Sample period is January 1, 2020 to August 7, 2020.

Economic Model Parameters

	BDRA-SSL	CRRA-SSL	BDRA	BDRA-SSL-C	BDRA-SIRD-SL
$A^U(s_t^m = e_1)$	-0.025679074	-0.026301739	0	-0.034872034	-0.028211856
$A^U(s_t^m = e_2)$	-0.000101566	-2.32016E-05	0	-6.35201E-06	-9.18794E-05
$A^U(s_t^m = e_3)$	-0.466881675	-1.87101006	0	-1.182054436	-0.469951409
$A^C(s_t^m)$	0.000465526	0.009732189	0	0.000791184	0.002305647
$A^D(s_t^m)$	0.001137158	0.002307249	0	0.004175592	0.004184565
a_i	0.99979819	0.503403821	1	0.999095977	0.888101087
a_l	0.999967397	0.533484811	1	0.999963014	0.999874155
ω	0.04120106	0.994271792	1	0.700019856	0.083317095
h	0.999786164	0.751741125	1	0.900225101	0.371829701

Pandemic Model Parameters

	BDRA-SSL	CRRA-SSL	BDRA	BDRA-SSL-C	BDRA-SIRD-SL
β_S	2.34542031	2.326128262	2.322575926	2.350291398	0.365428193
σ	0.063832594	0.067316419	0.076304487	0.064480039	0.090150029
γ	0.079741168	0.090294066	0.078438606	0.086906266	0.031253917
λ	0.018777052	0.007510959	0.021923334	0.018180779	0.087788844
λ_w	0.634122452	0.638395058	0.605927816	0.649034818	0.794464859
μ_i	0.0000222	0.0000222	0.0000222	0.0000222	0.0000222
ν^o	1.24892E-05	1.6264E-05	4.65216E-06	1.58571E-06	7.0138E-06
μ	0.0000056	0.0000056	0.0000056	0.0000056	0.0000056
κ_0 (pre SIP)	3.625968997	3.885362327	3.981425808	3.904037459	4.329844876
q	0.08026484	0.08161096	0.079885292	0.079729612	0.071758914
q_2	0.000620225	0.000739624	0.001005587	0.000600845	0.000311312
κ_1 (during SIP)	22.88789899	22.78483687	23.19114615	22.87036267	19.47293397
κ_2 (post SIP)	12.87719289	14.73788209	14.5132075	12.83753079	6.06472649
t_1	61.03122276	60.46892173	61.17339848	61.17140188	66.10591591
t_2	123.08807	123.7490243	119.9154812	123.047539	132.2162616
t_m	64.07840632	61.80245683	66.83447283	62.86362967	66.83447283
τ_0 (pre SIP)	12.28729912	17.25446367	21.4453125	15.10062809	5.024440623

Table 6: Model Specification Tests and Model Selection Criteria. Models are nested and non-nested. Specification tests are based on the quasi-log-likelihood ratio statistic $QLR_N = N(\widehat{J}_N - \widetilde{J}_N)$ statistic where N is the number of observations and $\widehat{J}_N$ ($\widetilde{J}_N$) is the constrained (unconstrained) quasi-log-likelihood function. The model selection criteria are $BIC = NJ_N - \frac{1}{2}np \ln N$ (Bayesian) resp. $AIC = NJ_N - np$ (Akaike) where J_N is the quasi-log-likelihood function and np is the number of model parameters.

Model	BDRA-SSL	BDRA-SSL-C	CRRA-SSL	BDRA	BDRA-SIRD-SL
# constr. param. (p)	unconstrained	4	2	9	non-nested
		Model Specifcation Tests			
QLR-statistic		949.3035	8638.2120	37233981.4565	
Critical value		5.9915	5.9915	16.9190	
p-value		0.0000	0.0000	0.0000	
		Model Selection Criteria			
BIC	2063.6955	3016.8492	10705.7577	37236062.4777	2099.1963
AIC	2107.1740	3058.4775	10747.3860	37236097.6305	2138.0494

The table also reveals that performance deteriorates substantially when the SSL pandemic component does not feed back into the economic model, as for the stripped model (BDRA). The main reason is because BDRA fails to capture the V-shaped pattern in the stock price adjustment. It also shows that the SSL model as well as BDRA are essential ingredients for good performance intra-pandemic. Figure 9 illustrates performance along one dimension, by displaying the volatility fits of the candidate models.

5. Conclusion

In this paper we extended the BDRA model to accommodate unpredictable pandemic events such as the onset of an outbreak and the discovery of a vaccine, as well as associated mitigating policies such as SIP and LIFT. The BDRA-SEIRD-SIP-LIFT model, called BDRA-SSL, was estimated using economic and disease data from the COVID-19 outbreak. The estimated model was found to provide a close fit to the realized trajectories of variables targeted in the estimation, i.e., the number of new cases, the S&P 500 level and the index return volatility. Model specification tests and model selection criteria show it dominates nested and non-nested alternatives such as BDRA, CRRA-SSL and BDRA-SIRD-SL during the pandemic. At the same time, it generated a close match to 25 unconditional moments of economic time series, hence displayed consistency with long run statistical properties of economic and financial time series. Beliefs-dependent risk aversion was found to be critical for explanations of phenomena pre- and intra-COVID-19 outbreak.

While the model developed provides a comprehensive explanation for long term and short term features of the data, it leaves room for further improvements. Among the phenomena that are not explained are the level and behavior of the short rate and of the term structure of interest rates, both in the long run and during the COVID-19 outbreak. In that regard, the average interest rate and bond yields generated by the model are too high, and short term fluctuations too large to properly capture the data. A critical ingredient for that purpose is likely to be monetary policy. Actions by the Federal Reserve, e.g., pertaining to the federal funds rate, have undoubtedly shaped the response of fixed income markets during the outbreak. More generally, Quantitative Easing has had a profound effect on these markets since its inception in 2008. Incorporating such monetary policies in the analysis is an avenue for future research.

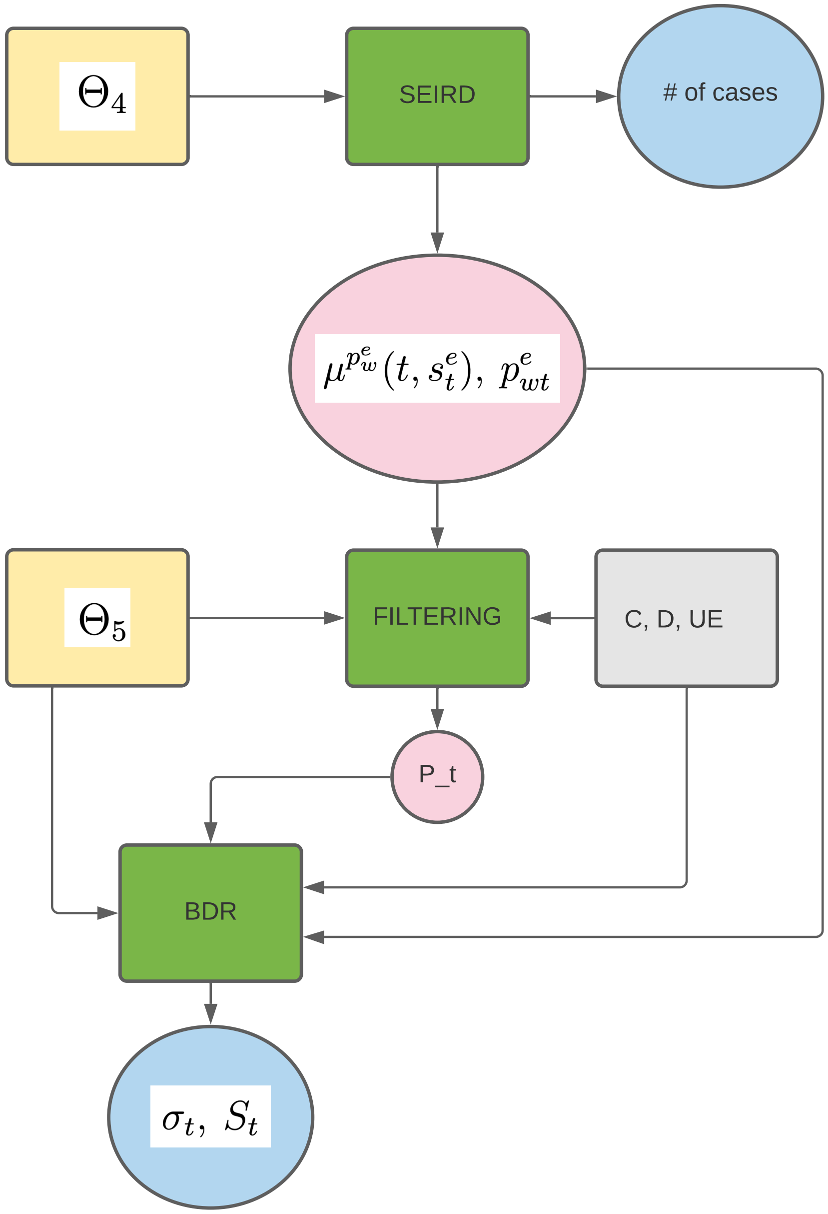

Figure 1: Estimation process diagram. Box colors are Yellow: parameters, Green: models, Grey: data, Pink: model output - intermediary quantities, Blue: model output - target quantities.

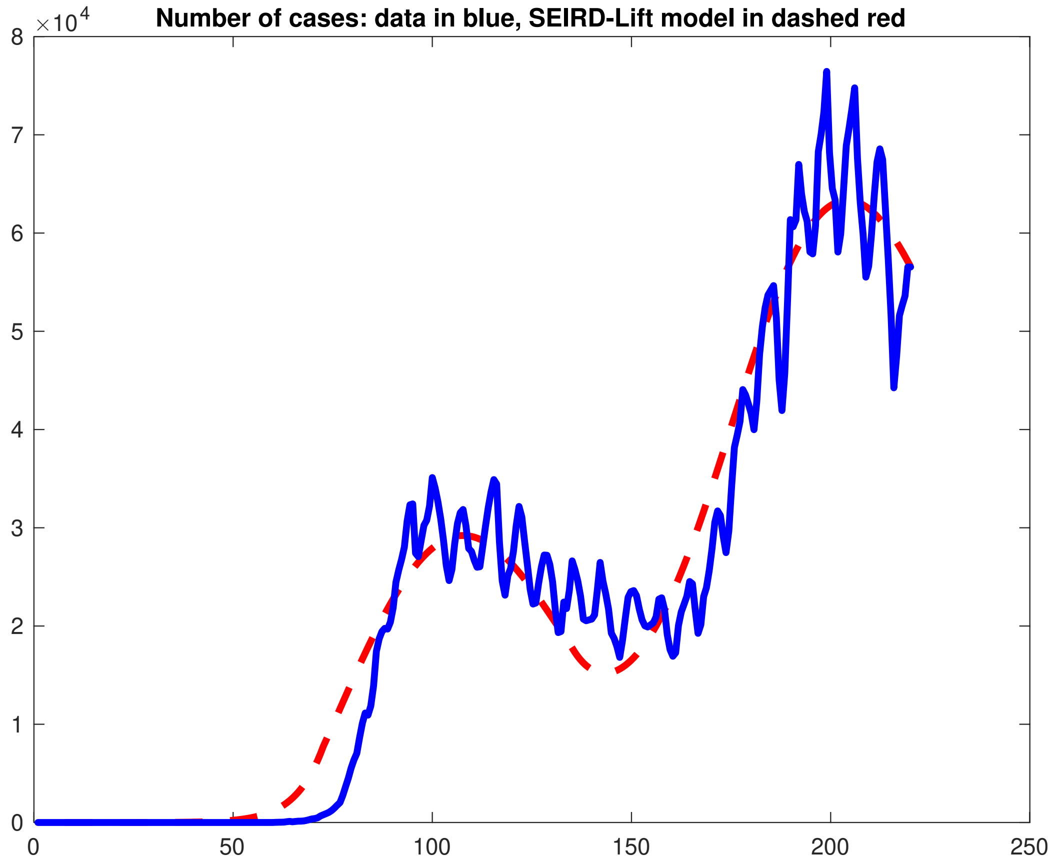

Figure 2: Number of cases in the data (solid blue) and in the BDRA-SSL model (dash red). The sample period is January 1st through August 7th. The x-axis displays the day number.

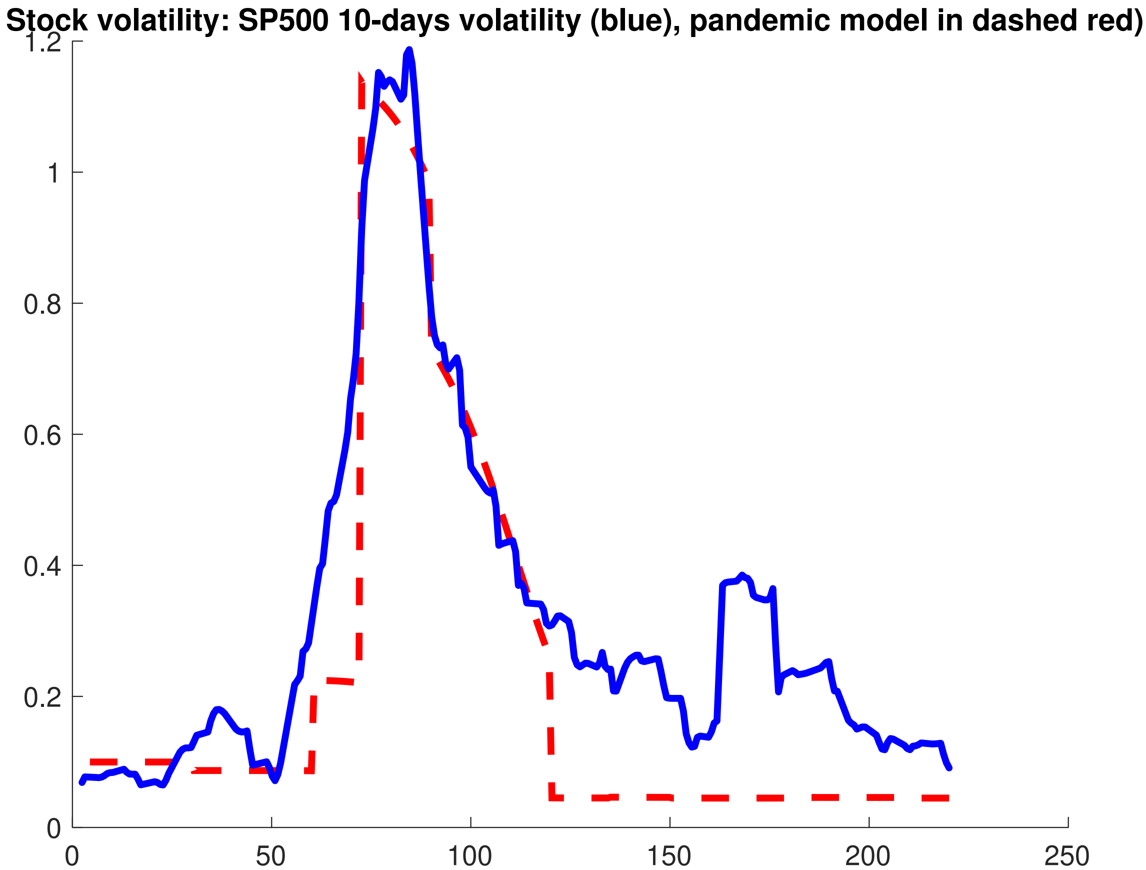

Figure 3: Stock price volatility: 10 days rolling volatility of the S&P500 (solid blue) and in the BDRA-SSL model (dash red). The sample period is January 1st through August 7th. The x-axis displays the day number.

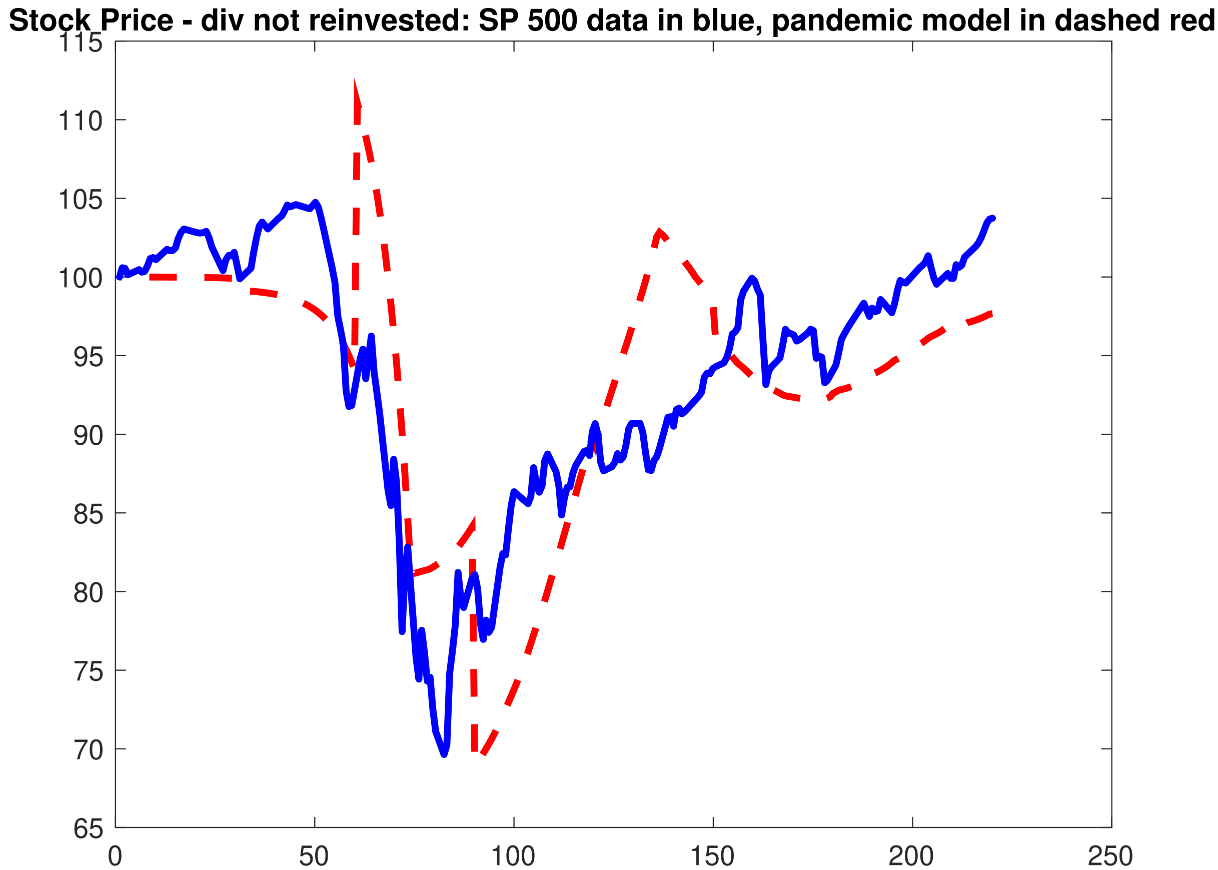

Figure 4: Stock price level: S&P500 dividend not reinvested (solid blue) and in the BDRA-SSL model (dash red). Prices are normalized at 100 on January 1st. The sample period is January 1st through August 7th. The x-axis displays the day number.

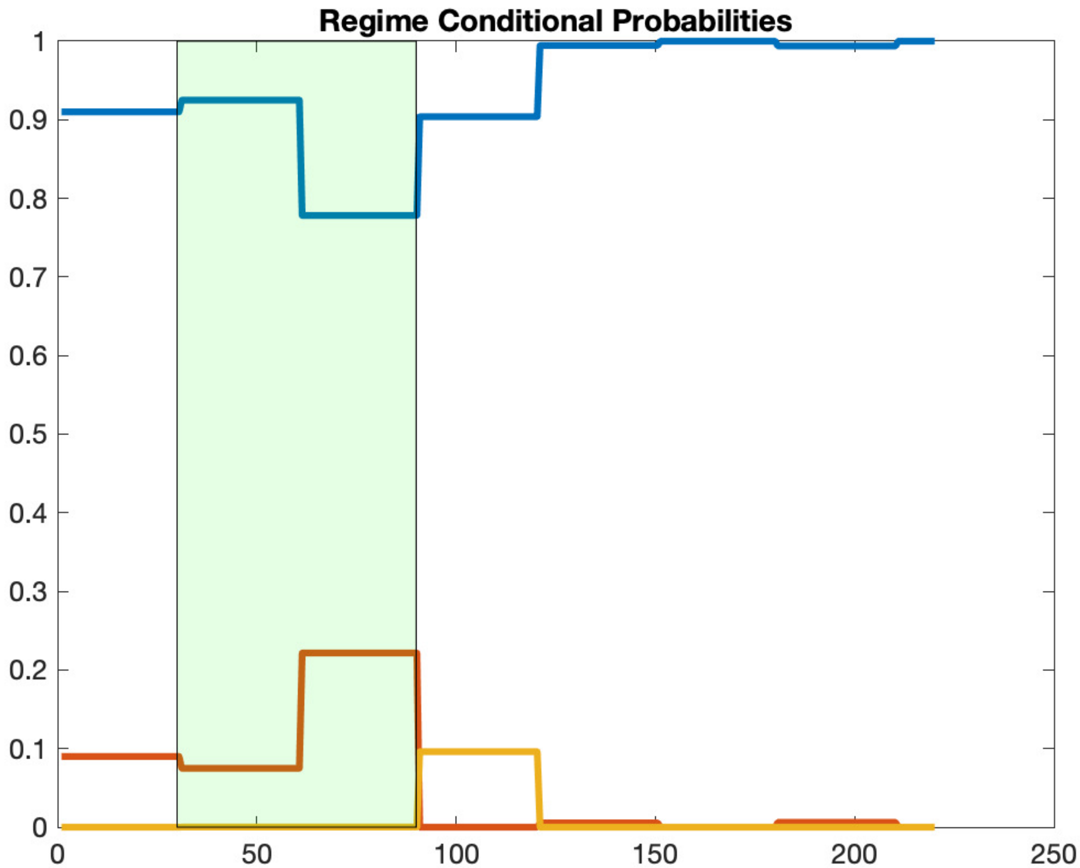

Figure 5: Conditional regime probabilities for the BDRA-SSL model. Normal regime in blue, Recession regime in red, Boom regime in yellow. The shaded area corresponds the NBER recession period. The sample period is January 1st through August 7th. The x-axis displays the day number.

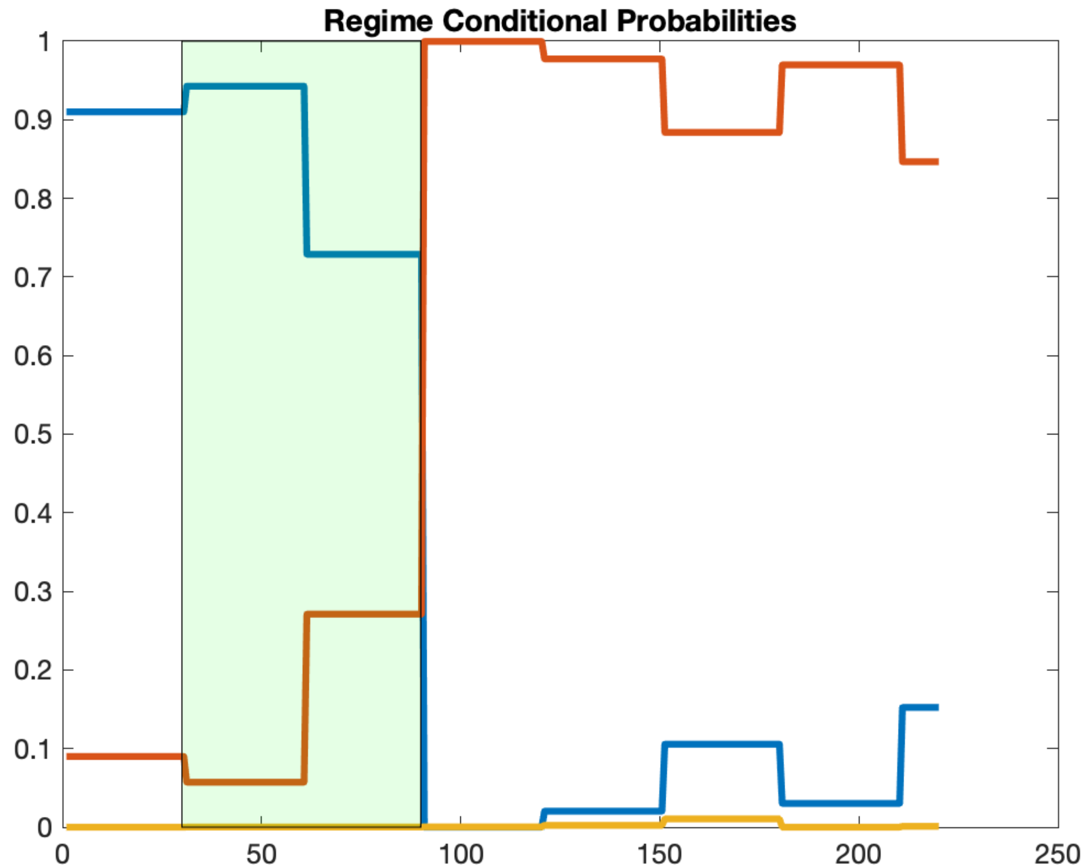

Figure 6: Conditional regime probabilities for the BDRA model without SSL. Normal regime in blue, Recession regime in red, Boom regime in yellow. The shaded area corresponds to the NBER recession period. The sample period is January 1st through August 7th. The x-axis displays the day number.

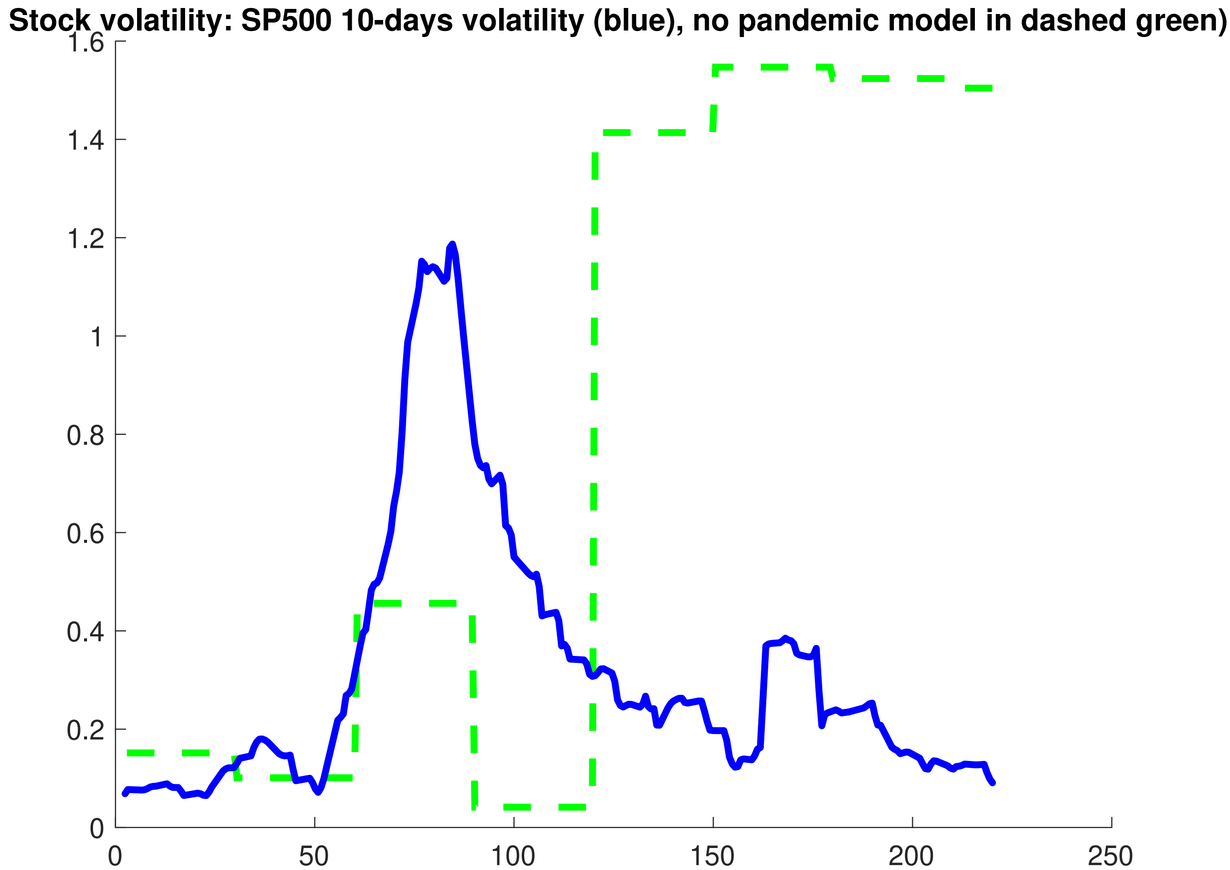

Figure 7: Volatility evolution in the data (solid blue) and the BDRA model without SSL (dash green). The sample period is January 1st through August 7th. The x-axis displays the day number.

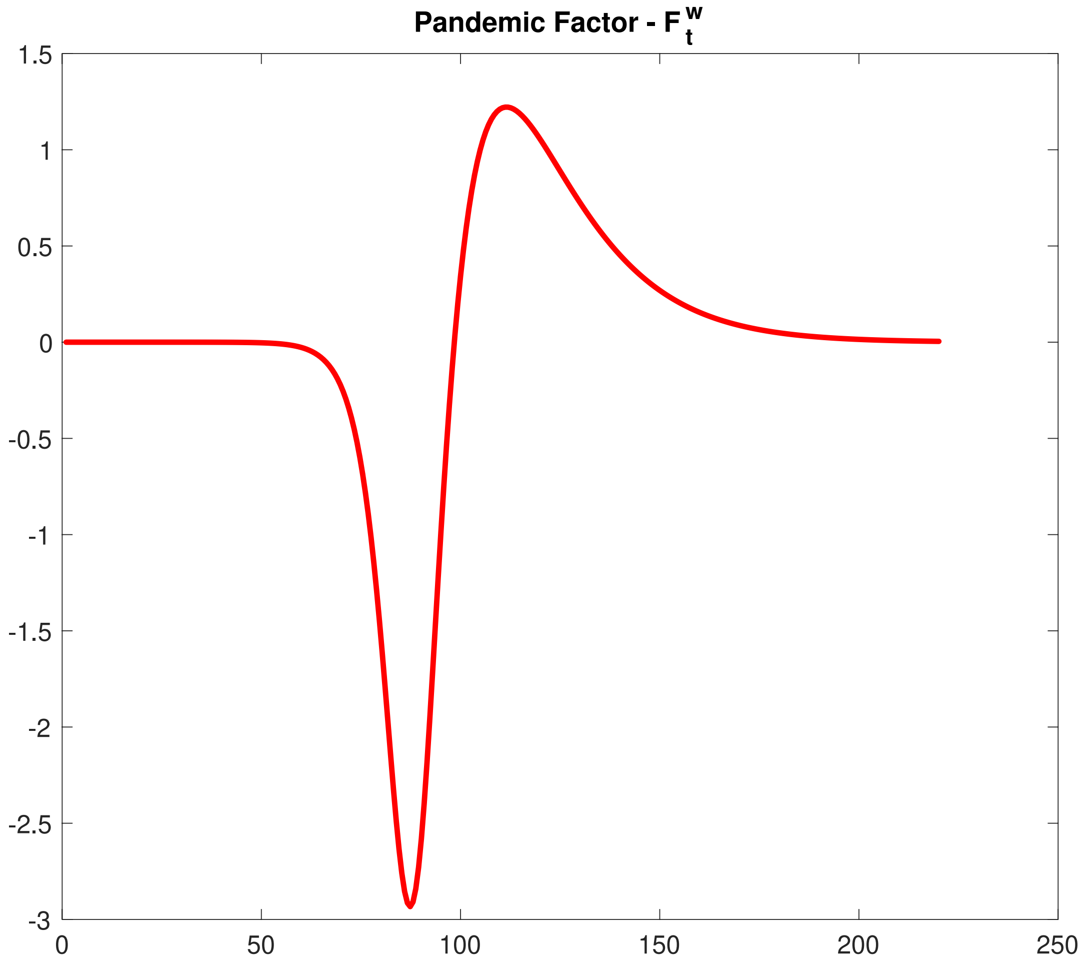

Figure 8: Evolution of pandemic factor F^w . The sample period is January 1st through August 7th. The x-axis displays the day number.

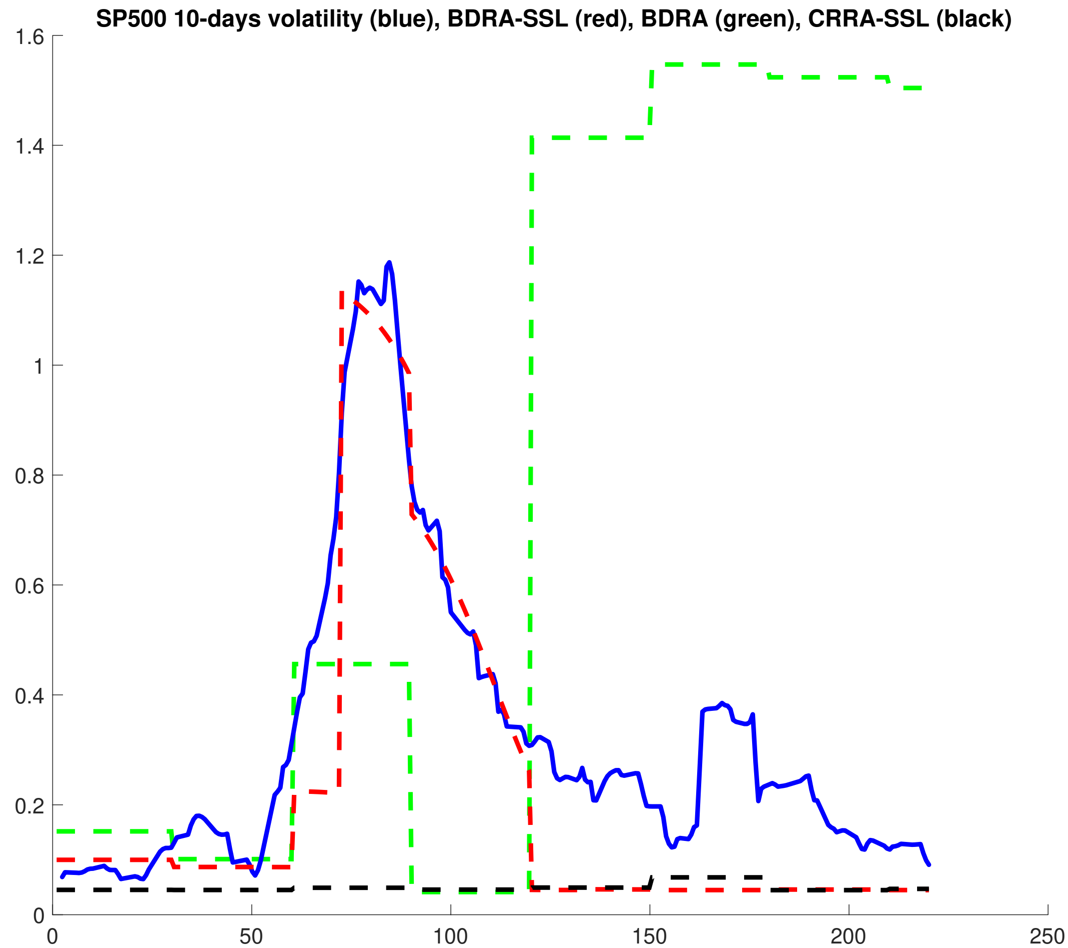

Figure 9: Comparative volatility evolution in the data (solid blue), BDRA-SSL (dash red), CRRA-SSL (dash black), and BDRA (dash green). The sample period is January 1st through August 7th. The x-axis displays the day number.

6. Appendix

6.1. Appendix A: the Stochastic SEIRD-SIP-LIFT Model

This appendix describes the SEIRD model under a SIP-LIFT policy, i,e,, a shelter-in-place (SIP) policy followed by a lifting (LIFT) of the restriction. Combining these three elements gives the SSL model. The SSL model developed here, extends Detemple (2022) by incorporating the unpredictable nature of pandemics and vaccine discoveries, captured by the Markov chain in Section 2.1. For generality we allow all the coefficients to be time-dependent.

In this model, populations in $\mathcal{S}, \mathcal{E}, \mathcal{I}$ transition to a sheltered stay-at-home state upon implementation of SIP and stay put until the policy is lifted. Sheltered (quarantined) populations are denoted with a superscript Q. Sheltered populations further split between work-at-home and laid-off populations, according to the fractions h, l where $h + 1 = 1$. Work-at-home and laid-off populations are subscripted by h and l, respectively. All infectious populations, sheltered and non-sheltered, split in three subgroups: asymptomatic, symptomatic mild, and symptomatic severe. Figure 6.1 illustrates the propagation mechanism across populations under SIP. Subgroups are not displayed.

We assume implementation of SIP takes time. The migration rate from $\mathcal{S}, \mathcal{E}, \mathcal{I}$ to the corresponding sheltered categories takes place at the constant rate q. Likewise when SIP is lifted, i.e., during LIFT, reverse migration from the sheltered categories to non-sheltered ones occurs at the constant rate q_2. In both cases, delays in implementation occur for a variety of reasons including the fact that policy recommendations are typically not uniformly adopted across states and, even when they are uniformly adopted, implementation may not be synchronous or instantaneous.

The evolution of populations in the SSL model is described by the following system of differential equations with stochastic component due to the unpredictable vaccine event

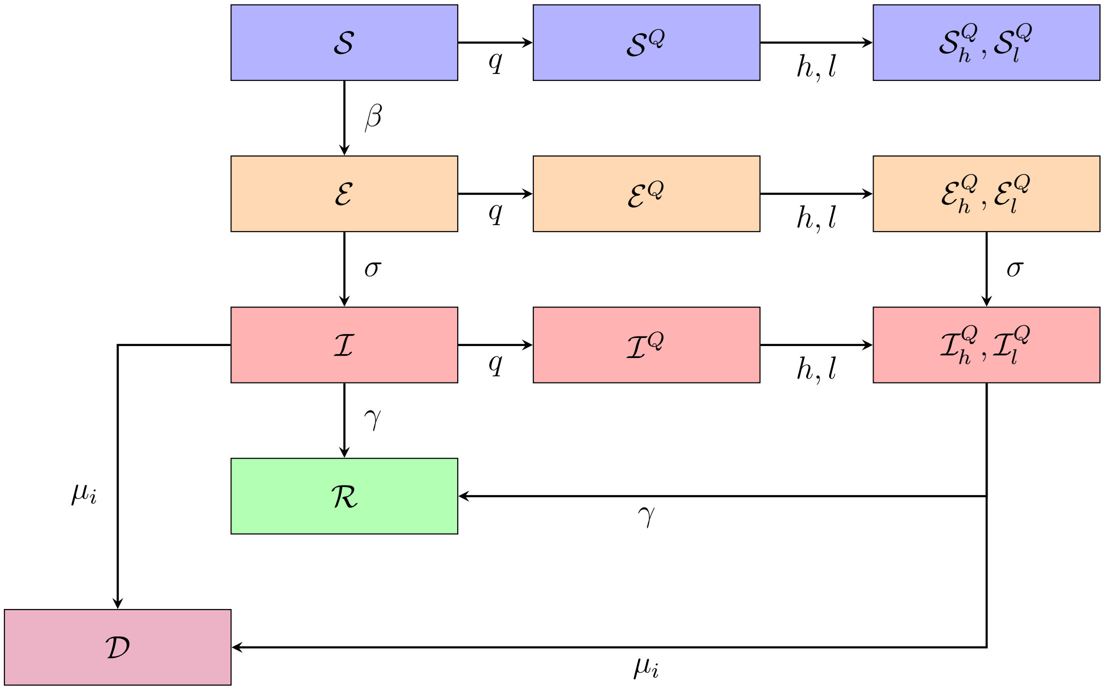

Figure 10: Flowchart for the SEIRD-SIP model.

$$
\begin{aligned}
dp_s &= (\mu_t(1 - p_d - p^Q_{s,h} - p^Q_{s,l} - p_s) - \beta_t p_i^{asy} p_s - (q_t + \nu_t^o + \nu_t 1_{\mathcal{V}_t}) p_s) dt \\
dp^Q_{s,h} &= (q_t h p_s - (\nu_t^o + \nu_t 1_{\mathcal{V}_t}) p^Q_{s,h}) dt \\
dp^Q_{s,l} &= (q_t (1-h) p_s - (\nu_t^o + \nu_t 1_{\mathcal{V}_t}) p^Q_{s,l}) dt \\
dp_e &= (\beta_t p_i^{asy} p_s - (q_t + \mu_t + \sigma_t) p_e) dt \\
dp^Q_{e,h} &= (q_t h p_e - (\mu_t + \sigma_t) p^Q_{e,h}) dt \\
dp^Q_{e,l} &= (q_t (1-h) p_e - (\mu_t + \sigma_t) p^Q_{e,l}) dt \\
dp_i &= (\sigma_t p_e - (q_t + \mu_t + \mu_{it} + \gamma_t) p_i) dt \\
dp^Q_{i,h} &= (q_t h p_i + \sigma_t p^Q_{e,h} - (\mu_t + \mu_{it} + \gamma_t) p^Q_{i,h}) dt \\
dp^Q_{i,l} &= (q_t (1-h) p_i + \sigma_t p^Q_{e,l} - (\mu_t + \mu_{it} + \gamma_t) p^Q_{i,l}) dt \\
dp_r &= (\gamma_t (p_i + p^Q_{i,h} + p^Q_{i,l}) - \mu_t p_r + (\nu_t^o + \nu_t 1_{\mathcal{V}_t})(p_s + p^Q_{s,h} + p^Q_{s,l})) dt \\
dp_d &= \mu_{it} (p_i + p^Q_{i,h} + p^Q_{i,l}) dt
\end{aligned}
\tag{6.1}
$$

Several additional aspects of the propagation model under SIP are worth highlighting. First, all births are assigned to the susceptible classes. For sheltered susceptible $\mathcal{S}^Q$, as the birth rate equals the death rate, natural growth is null. For non-sheltered susceptible $\mathcal{S}$, natural growth is determined by the excess of birth in the surviving population $1 - p_d$ net of birth assigned to the sheltered susceptible p_s^Q over death in the non-sheltered susceptible p_s . Aggregating over sheltered and non-sheltered populations gives a flow of birth equal to $(1 - p_d)\mu$. Second, populations in $\mathcal{S}^Q$ remain isolated, until the policy is lifted or they transition to $\mathcal{R}$ due to natural immunity or vaccination. Hence, they cannot be contaminated during that period. Third, $\mathcal{R}$ includes all recovered, naturally immune and vaccinated populations. Such individuals are immune to the disease, therefore apt to rejoin the workforce.[9] Fourth, $\mathcal{D}$ includes all the deceased from an infection: the fraction p_d is the cumulative death toll as a fraction of the initial population $p_0 = 1$. Last, the transition from $\mathcal{S}$ to $\mathcal{E}$ does not depend on sheltered individuals. Contamination, in fact, is entirely driven by non-sheltered asymptomatic individuals.

As previously indicated, lifting SIP, i.e., applying LIFT, reverses the migrations from $\mathcal{S}, \mathcal{E}, \mathcal{I}$ to $\mathcal{S}^Q, \mathcal{E}^Q, \mathcal{I}^Q$ in the model above. The negative of the reverse compliance rate $-q_2$ replaces q . Applying that rate to sheltered symptomatic infectious populations does not affect the economic properties of the model, because such populations are not able to work by assumption.

6.2. Appendix B: Proofs

Proof of Proposition 2.1. The first order condition for population $j \in \{s, e, i, r\}$ is

$$\sum_{k=1}^{K} P_k \left(\frac{c_t}{a_j} \right)^{-R_k} = \frac{y\xi_t}{a_t} \equiv H_t. \tag{6.2}$$

where y is a constant Lagrange multiplier, ξ_t is the stochastic discount factor and $a_t = e^{-\beta_u t}$ is the subjective discount factor. Optimal consumption is $c_t = a_j I(H_t)$ where the function I ,

[9]The formulation abstracts from issues of incomplete information pertaining to the health status of populations, in particular asymptomatic infectious ones.

by concavity and Inada conditions, is the unique solution of the equation $\sum_{k=1}^{K} P_k I^{-R_k} = H$ and is independent of j.

Equilibrium in the consumption good market ensures $\sum_{j\in\{s,e,i,r\}} p_j a_j I(H_t) = C_t$. Solving gives $I(H_t) = C_t/p^a_c$ with $p^a_c = \sum_{j\in\{s,e,i,r\}} p_j a_j$. Hence, up to a constant, the stochastic discount factor is

$$(6.3) \qquad \xi_t = \sum_{k=1}^{K} e^{-\beta_u t} \left(\frac{C_t}{p^a_{ct}}\right)^{-R_k} P_{kt}.$$

The jump in the SDF at $t = \tau_0$ is

$$(6.4) \qquad \frac{\Delta\xi_t}{\xi_{t-}} = \sum_{k=1}^{K} \frac{e^{-\beta_u t} C_t^{-R_k} P_{kt}}{\sum_{k=1}^{K} e^{-\beta_u t} C_t^{-R_k} P_{kt}} \left((p^a_{ct})^{R_k} - 1 \right) dN^e_{12,t}$$

where $p^a_{ct} = 1 + \Delta_i(\lambda_i + \lambda_s a_i - 1)$ and Δ_i is the jump in p_{it}, and where we used $p^a_{ct-} = 1$. The coefficient $\lambda_s = (1-\lambda)(1-\lambda_w)$ is the fraction of symptomatic mild in the infectious population, $\lambda_i = (1-\lambda)\lambda_w$ is the fraction of asymptomatic. The jump in the SPD at $t = \tau_1$ is null because p^a_c is continuous at that point

Given the observed filtration, the SPD has dynamics,

$$d\xi_t/\xi_{t-} = -r_{t-}dt - \sum_{\alpha\in\{C,G,Y\}} \theta^\alpha_{t-} d\nu^\alpha_t - \theta^{e_2}_{t-} d\tilde{N}^e_{12,t}.$$

where r is the interest rate, θ^α_t for $\alpha \in \{C, G, Y\}$ is the market price of risk associated with the innovations $d\nu^\alpha_t = dW^\alpha_t - \sum_{k=1}^{3} \mu^\alpha(e_k) P_{kt} dt$, $d\tilde{N}^e_{ij,t} = dN^e_{ij,t} - \Lambda^e_{ij} dt$ are the jump innovations and $\theta^{e_j}_t$ are the market prices of jump risks. Taking derivatives on both sides of (6.3) and identifying drift, jump, and volatility coefficients for diffusion and jump risks yields the formulas announced. In particular,

$$(6.5) \qquad \theta^{e_2}_{t-} = \sum_{k=1}^{K} \frac{e^{-\beta_u t} C_t^{-R_k} P_{kt}}{\sum_{k=1}^{K} e^{-\beta_u t} C_t^{-R_k} P_{kt}} \left(1 - (p^a_{ct})^{R_k}\right)$$

and $\theta^{e_3}_{t-} = 0$. The interest rate has the jump premium component $\theta^{e_2}_{t-} \Lambda_{12}$. □

Proposition 6.1. *Define* $H_{kt}^B \equiv e^{-\beta_k t} (p_{ct}^a)^{R_k} C_t^{-R_k}$, $(H_t^B)' = [H_{1t}^B, \cdots, H_{Kt}^B]$ *and the state variable* $Z_t = (H_t^B)' / \left(H_t^B\right)' P_t$ *. The price-dividend ratio is* $S_t/D_t = Z_t' \Upsilon(t) P_t$ *where the* $K^2 \times K^2$ *matrix* $\Upsilon(t)$ *is defined in (6.9).*

Proof of Proposition 6.1. Define the stopping times $\tau_1 = \inf\{t : s_t^e = e_2\}$ and $\tau_2 = \inf\{t : s_t^e = e_3\}$ and note that on the interval $t \in (0, \tau_1) \equiv \mathcal{T}_1$, $s_t^e = e_1$, on $t \in [\tau_1, \tau_2) \equiv \mathcal{T}_2$, $s_t^e = e_2$, and on $t \in [\tau_2, \infty) \equiv \mathcal{T}_3$, $s_t^e = e_3$. The time partition $\{\mathcal{T}_1, \mathcal{T}_2, \mathcal{T}_e\}$ will be used to show that $E_t \left[\xi_v D_v | \tau_1, \tau_2\right] = Z_t' \Upsilon^S(t, v, s_t^e, \tau_1, \tau_2) P_t$ where Z is an observed state variable. The stock price and price dividend ratio are then obtained by integrating over the densities of the switching times. Note that on each sub-interval $\mathcal{T}_j$, $s_t^e = e_j$ and the population weights in the SSL model are deterministic functions of time, switching times and their known initial values.

Using $D_t = C_t^\kappa G_t$ (see Appendix C), define $H_{kt} \equiv e^{-\beta_k t} (p_{ct}^a)^{R_k} C_t^{-R_k} D_t = H_{kt}^B D_t = e^{-\beta_k t} (p_{ct}^a)^{R_k} C_t^{\kappa - R_k} G_t$ and the vectors $H_t' = [H_{1t}, \cdots, H_{Kt}]$ and $(H_t^B)' = [H_{1t}^B, \cdots, H_{Kt}^B]$. The state price density is $\xi_t = y \xi_t^u$ with $\xi_t^u = \left(H_t^B\right)' P_t$ and y constant. Then define the filtration augmented by the switching times $\mathbb{G} = \mathbb{F} \bigvee \sigma(\tau_1, \tau_2)$, the conditional expectation $M_{t,v} \equiv E\left[\xi_v^u D_v | \mathcal{G}_t\right]$ for arbitrary $v > \tau_2$ and conjecture $M_{t,v} = N_{t,v}$ where $N_{t,v} \equiv \left(D_t H_t^B\right)' \Upsilon^S(t, v, s_t^e, \tau_1, \tau_2) P_t$ for $t \leqslant v$, with boundary condition $M_{v,v} = \xi_v^u D_v = \left(D_v H_v^B\right)' P_v$, i.e., $\Upsilon^S(v, v, \cdot, \cdot, \cdot) = I_K$, the $K \times K$ identity matrix. Next, note that all drift and diffusion coefficients depend on s_t^e only through τ_1, τ_2 . It follows that Υ^S is a function of t, v, τ_1, τ_2 only. If the conjecture is true, then $N_{t,v} \left(D_t H_t^B\right)' \Upsilon^S(t, v, \tau_1, \tau_2) P_t$ must be a $\mathbb{G}$ -martingale.

First, P is continuous, and H is continuous except at $t = \tau_1$ where p_c^a jumps. As $P_t = P_{t-}$, $H_t = H_{t-}$ for $t \neq \tau_1$ and $H_t' = H_{t-}' \mathrm{diag}\left[(p_{ct}^a)^{R_k}\right]$ at $t = \tau_1$, we then obtain

$$
\begin{aligned}
\Delta N_{t,v} = (H_{t-})' &\left(\left(\mathrm{diag}\left[p_{ct}^{R_k}\right] \Upsilon^S(t, v, \tau_1, \tau_2) - \Upsilon^S(t-, v, \tau_1, \tau_2) \right) 1_{t=\tau_1} \right) P_{t-} \\
&+ (H_{t-})' \left(\left(\Upsilon^S(t, v, \tau_1, \tau_2) - \Upsilon^S(t-, v, \tau_1, \tau_2) \right) 1_{t=\tau_2} \right) P_{t-} \\
&+ (H_{t-})' \left(\left(\Upsilon^S(t, v, \tau_1, \tau_2) - \Upsilon^S(t-, v, , \tau_1, \tau_2) \right) 1_{t\neq\tau_1, t\neq\tau_2} \right) P_{t-}.
\end{aligned}
$$

Second, the martingale $M_{t,v}$ can be decomposed into a continuous and discontinuous part:

$M_{t,v} = M^c_{t,v} + M^d_{t,v}$. The jumps in the discontinuous part $M^d_{t,v}$ only depend on the jumps in the regime indicator s^e_t . However, as in $\mathbb{G}$ the jump times and therefore the increments Δs^e_t are known, it follows that $\Delta M_{t,v} = 0$. If the conjecture holds, it must therefore be the case that $\Delta N_{t,v} = 0$, implying $\Upsilon^S(t, v, \tau_1, \tau_2)$ is continuous for $t \in \mathcal{T}_j$ and at the boundaries,

$$\begin{aligned}\Upsilon^S(\tau_1-, v, \tau_1, \tau_2) =& \text{diag}\left[\left(p^a_{c\tau_1}\right)^{R_k}\right]\Upsilon^S(\tau_1, v, \tau_1, \tau_2)\\ \Upsilon^S(t-, v, \tau_1, \tau_2) =& \Upsilon^S(t, v, \tau_1, \tau_2) \quad \text{for all} \quad t \neq \tau_1.\end{aligned}$$

Ito's formula and the $\mathbb{G}$ -martingale property then imply

$$\begin{aligned}-(H_t)'\frac{\partial \Upsilon^S(t, v, \tau_1, \tau_2)}{\partial t}P_t =& (H_t)'\left(\left(\mu^H_t\right)'\Upsilon^S(t, v, \tau_1, \tau_2) + \Upsilon^S(t, v, \tau_1, \tau_2)\Lambda'\right)P_t\\ &+ (H_t)'\left(\sum_{\alpha\in\{C,G\}}\left(\sigma^{H,\alpha}_t\right)'\Upsilon^S(t, v, \tau_1, \tau_2)\,\sigma^{\alpha,P}_t\right)P_t\end{aligned}$$

where, with $\gamma_k = \kappa - R_k$,

$$\begin{aligned}\sigma^{\alpha,P}_t &= \text{diag}\left[\frac{\mu^\alpha_{kt} - \widehat{\mu}^\alpha_t}{\sigma^\alpha}\right], \qquad \sigma^{H,C}_t = \text{diag}\left[\gamma_k\right]\sigma^C, \qquad \sigma^{H,G}_t = \sigma^G I_K\\ \mu^H_t &= -\text{diag}\left[\beta_k - \gamma_k\widehat{\mu}^C_t - R_k F^a_t 1_{\{t\geqslant\tau_1\}} - \frac{1}{2}\gamma_k(\gamma_k - 1)\left(\sigma^C\right)^2\right] + \widehat{\mu}^G_t I_K\\ \widehat{\mu}^\alpha_t &= \sum_{k=1}^K \mu^\alpha_{kt}P_{kt}; \quad \widehat{A}^\alpha_t = \sum_{k=1}^K A^\alpha_k P_{kt}; \quad \mu^\alpha_{kt} = \mu^\alpha_{ok} + A^\alpha_k F^w_t 1_{\{t\geqslant\tau_1\}} \quad \alpha \in \{C, G\}\\ F^w_t &= F^w(t, \tau_1, \tau_2) = \frac{\mu^{p^e_w}_t}{p^e_{wt}}; \quad \mu^{p^e_w}_t = \mu^{p^e_w}(t, \tau_1, \tau_2); \quad p^e_{wt} = p^e_w(t, \tau_1, \tau_2)\\ F^a_t &= F^a(t, \tau_1, \tau_2) = \frac{\mu^{p^a_c}_t}{p^a_{ct}}; \quad \mu^{p^a_c}_t = \mu^{p^a_c}(t, \tau_1, \tau_2); \quad p^a_{ct} = p^a_c(t, \tau_1, \tau_2)\\ \mu^\alpha_k&(t, \tau_1, \tau_2) = \mu^\alpha_{ok} + A^\alpha_k F^w(t, \tau_1, \tau_2)1_{t\geqslant\tau_1}.\end{aligned}$$

Cancelling terms on the RHS in the first and second lines shows that if Υ^S solves the ODE,

$$-\frac{\partial}{\partial t}\Upsilon^S(t, v, t_1, t_2) = \text{diag}[g_k(t, t_1, t_2)]\Upsilon^S(t, v, t_1, t_2) + \Upsilon^S(t, v, t_1, t_2)\Lambda'$$

$$+ \operatorname{diag}[\gamma_k]\Upsilon^S(t,v,t_1,t_2)\operatorname{diag}[\mu_k^C(t,t_1,t_2)]$$
$$+ \Upsilon^S(t,v,t_1,t_2)\operatorname{diag}[\mu_k^G(t,t_1,t_2)]$$

with boundary conditions $\Upsilon^S(v-,v,t_1,t_2) = I_K$ for $t \in [t_1,v)$, $\Upsilon^S(t_2-,v,t_1,t_2) = \Upsilon^S(t_2,v,t_1,t_2)$ for $t \in [t_1,t_2)$, and $\Upsilon^S(t_1-,v,t_1,t_2) = \operatorname{diag}\left[\left(p^a_{ct_1}\right)^{R_k}\right]\Upsilon^S(t_1,v,t_1,t_2)$ for $t \in (0,t_1)$, where

$$g_k(t,t_1,t_2) \equiv -\beta_k + \frac{1}{2}\gamma_k(\gamma_k-1)\left(\sigma^C\right)^2 + R_k F^a(t,t_1,t_2)1_{\{t\geqslant t_1\}},$$

then indeed $M_{t,v} = \left(D_t H_t^B\right)'\Upsilon^S(t,v,\tau_1,\tau_2)P_t$ for $t \leqslant v$.

Integrating over v then gives with $\upsilon(t,t_1,t_2) \equiv \int_t^\infty \Upsilon^S(t,v,t_1,t_2)dv$,

$$-\frac{\partial}{\partial t}\upsilon(t,t_1,t_2) = I_{K^2} + \operatorname{diag}[g_k(t,t_1,t_2)]\upsilon(t,t_1,t_2) + \upsilon(t,t_1,t_2)\left(\Lambda' + \operatorname{diag}[\mu_k^G(t,t_1,t_2)]\right)$$
$$+ \operatorname{diag}[\gamma_k]\upsilon(t,t_1,t_2)\operatorname{diag}[\mu_k^C(t,t_1,t_2)]$$

with boundary condition, $[\upsilon(\infty,t_1,t_2)]_{ij} = \left(e_i' \otimes e_j'\right)\left[-\overline{\Upsilon}^{-1}\right]\operatorname{vec}(I_{K^2})$ for $t \in [t_1,\infty)$, and $\upsilon(t_1-,t_1,t_2) = \operatorname{diag}\left[\left(p^a_{ct_1}\right)^{R_k}\right]\upsilon^S(t_1,t_1,t_2)$ for $t \in (0,t_1)$, where[10]

$$\overline{\Upsilon} \equiv I_{K^2} \otimes \operatorname{diag}[\overline{g}_k] + \left(\Lambda + \operatorname{diag}[\mu_{ok}^G]\right) \otimes I_{K^2} - \operatorname{diag}[\mu_{ok}^C] \otimes \operatorname{diag}[\gamma_k] \tag{6.6}$$
$$\overline{g}_k \equiv -\beta_k + \frac{1}{2}\gamma_k(\gamma_k-1)\left(\sigma^C\right)^2. \tag{6.7}$$

Define $Z_t = H_t^B / \left(H_t^B\right)' P_t$ and assume the largest eigenvalue of $-\overline{\Upsilon}$ is negative. We then get

$$S_t = \frac{E_t\left[\int_t^\infty \left(H_v^B\right)' P_v D_v dv\right]}{\left(H_t^B\right)' P_t} = D_t Z_t' \Upsilon(t) P_t \tag{6.8}$$

[10]The Kronecker product of matrices A and B , of dimensions $K_1 \times K_2$ and $L_1 \times L_2$, is the matrix $A \otimes B = [A_{ij}B]$ of dimension $(K_1 \times L_1) \times (K_2 \times L_2)$ where each element of A is multiplied by matrix B .

where

$$
\Upsilon(t)=\begin{cases} \upsilon\left(t,\tau_1,\tau_2\right) & t\geqslant\tau_2 \\ \int_t^\infty \upsilon\left(t,\tau_1,y\right)\lambda_{23}^e e^{-\lambda_{23}^e(y-t)}dy & t\in[\tau_1,\tau_2) \\ \int_t^\infty\int_x^\infty \upsilon\left(t,x,y\right)\lambda_{12}^e\lambda_{23}^e e^{-\lambda_{12}^e(x-t)-\lambda_{23}^e(y-x)}dydx & t\in[0,\tau_1) \end{cases}. \tag{6.9}
$$

This completes the proof. □

6.3. Appendix C: Orthogonalization

The state variables $X_t'\equiv[C_t,G_t,Y_t]$ are orthogonalized state variables derived from macro variables $\widetilde{X}_t\equiv[C_T,D_t,U_t]$, where C_t is per capita consumption, D_t aggregate dividends, and U_t unemployment. Macro state variables have covariance matrix Σ and dynamics

$$
d\widetilde{X}_t=\text{diag}[\widetilde{X}_t]\left(\left(\overline{\mu}^{\tilde{X}}s_t^m+\widetilde{A}(s_t^m)F_t^w 1_{\mathcal{E}_t}\right)dt+\Sigma dW_v\right) \tag{6.10}
$$

where $\widetilde{A}'(s_t^m)=[A^C(s_t^m),A^D(s_t^m),A^U(s_t^m)]$, $\overline{\mu}^{\tilde{X}}$ is a 3×3 matrix with rows given by expected growth rates, Σ is the Choleski decomposition of the covariance matrix $\Sigma\Sigma'$,

$$
\overline{\mu}^{\tilde{X}}=\begin{bmatrix}\mu_1^C & \mu_2^C & \mu_3^C\\ \mu_1^D & \mu_2^D & \mu_3^D\\ \mu_1^U & \mu_2^U & \mu_3^U\end{bmatrix},\ \Sigma\equiv\begin{bmatrix}\sigma^C & 0 & 0\\ \rho^{CD}\sigma^D & \sqrt{1-(\rho^{CD})^2}\sigma^D & 0\\ \rho^{CU}\sigma^U & \rho^{DU}\sigma^U & \sqrt{1-(\rho^{CU})^2-(\rho^{DU})^2}\sigma^U\end{bmatrix},
$$

and $W_t'=\left[W^C,W^G,W^Y\right]$ is a 3 -dimensional vector of independent Brownian motions.

To find the orthogonalized state variables, define $\widetilde{x}_{it}=\log\widetilde{X}_{it}$ and note that

$$
d\widetilde{x}_t=\left(\overline{\mu}^{\tilde{X}}s_t^m-\frac{1}{2}\text{dg}\left[\Sigma\Sigma'\right]+A(s_t^m)F_t^w 1_{\mathcal{E}_t}\right)dt+\Sigma dW_t
$$

where for a $m\times m$ square matrix B , $\text{dg}[B]$ is the $m\times1$ vector of diagonal elements of B .

Then define $\widehat{x}_t = K\widetilde{x}_t$ with $K = \text{diag}[\text{dg}[\Sigma]]\Sigma^{-1}$ and note that

$$d\widehat{x}_t = K\left(\overline{\mu}^{\tilde{X}} s_t^m - \frac{1}{2}\text{dg}\left[\Sigma\Sigma'\right] + \widetilde{A}(s_t^m)F_t^w 1_{\mathcal{E}_t}\right)dt + \text{diag}[\text{dg}[\Sigma]]dW_t.$$

Finally, set $X_t = \exp\left(\widehat{x}_t\right)$ and note that

$$dX_t = \text{diag}[X_t]\left(\mu^X(t, s_t^m, s_t^e)dt + \text{diag}[\text{dg}[\Sigma]]dW_t\right) \tag{6.11}$$

$$\mu^X(t, s_t^m, s_t^e) = K\left(\overline{\mu}^{\tilde{X}} s_{t-}^m - \frac{1}{2}\text{dg}\left[\Sigma\Sigma'\right] + \widetilde{A}(s_t^m)F_t^w 1_{\mathcal{E}_t}\right) + \frac{1}{2}\text{dg}[\text{dg}[\Sigma]\text{dg}[\Sigma]']. \tag{6.12}$$

This establishes the one-to-one mapping between underlying and orthogonalized macro factors in (2.8), (2.9), (2.10). With $A(s_t^m) = \left[A^C(s_t^m), A^G(s_t^m), A^Y(s_t^m)\right]$, the relations are $A(s_t^m) = K\widetilde{A}(s_t^m)$, $\mu_o^X(s_t) = K\left(\mu^{\tilde{X}} s_{t-} - \frac{1}{2}\text{dg}\left[\Sigma\Sigma'\right]\right) + \frac{1}{2}\text{dg}[\text{dg}[\Sigma]\text{dg}[\Sigma]']$ and $\Sigma_{ij}^X = 1_{\{i=j\}}\text{dg}[\Sigma]_i$. The last relation shows $\sigma^C = \sigma^C$, $\sigma^G = \sigma^D\sqrt{1-(\rho^{CD})^2}$ and $\sigma^Y = \sigma^U\sqrt{1-(\rho^{CU})^2-(\rho^{DU})^2}$.

References

[1] Berrada, T., Detemple, J. and M. Rindisbacher (2018). Asset Pricing with Beliefs-Dependent Risk Aversion and Learning. *Journal of Financial Economics* 128(3), 504–534.

[2] Beeler, J. and J.Y. Campbell (2012). The Long-run Risks Model and Aggregate Asset Prices: an Empirical Assessment. *Critical Finance Review* 1(1), 141–182.

[3] Breeden, D.T. (1979). An Intertemporal Asset Pricing Model with Stochastic Consumption and Investment Opportunities *Journal of Financial Economics* 7(3), 265-296.

[4] Campbell, J.Y. and R.J. Shiller (1988). The Dividend-Price Ratio and Expectations of Future Dividends and Discount Factors. *Review of Financial Studies* 1(3), 195–228.

[5] Cheng. I.H. (2020). Volatility Markets Underreacted to the Early Stages of the COVID-19 Pandemic. *Review of Asset Pricing Studies* 10(4), 635–668.

[6] The COVID Tracking Project. https://covidtracking.com/data/national

[7] Cox, J.C., Ingersoll, J.E. and S.A. Ross (1985). A Theory of the Term Structure of Interest Rates, *Econometrica* 53(2), 385–407.

[8] Detemple, J. (2022). Asset Prices and Pandemics: The Effects of Lockdowns. *Quarterly Journal of Finance* 12(1), 2240002.

[9] Eichenbaum, M.S., Rebelo, S. and M. Trabandt (2021). The Macroeconomics of Epidemics. *Review of Financial Studies* 34(11), 5149–5188.

[10] Gormsen, N.J. and R.S.J. Koijen (2020). Coronavirus: Impact on Stock Prices and Growth Expectations, *Review of Asset Pricing Studies* 10(4), 574–597.

[11] Harvey, C.R. (1988). The Real Term Structure and Consumption Growth. *Journal of Financial Economics* 22(2), 305–333.

[12] Hong, H., Wang, N. and J. Yang (2021). Implications of Stochastic Transmission Rates for Managing Pandemic Risks. *Review of Financial Studies* 34(11): 5224–5265.

[13] Jones, C.J., Philippon, T. and V. Venkateswaran (2021). Optimal Mitigation Policies in a Pandemic: Social Distancing and Working from Home. *Review of Financial Studies* 34(11): 5188–5223.

[14] Merton, R.C. (1973), An Intertemporal Capital Asset Pricing Model. *Econometrica* 41(5), 867-887.

[15] Ogaki, M. (1993). Generalized Method of Moments: Econometric Applications. *Handbook of Statistics* 11, 455–488.

[16] Politis, D.N. and J.P. Romano (1994). Large Sample Confidence Regions Based on Subsamples under Minimal Assumptions. *Annals of Statistics* 22(4), 2031–2050 .